A MICROWAVE SPECTROMETER FOR THE STUDY OF SPIN-LATTICE RELAXATION EFFECTS AT LOW TEMPERATURES

A Thesis

presented by

R. Alan Beveridge, B.Sc.

to the

University of St Andrews

in application for the Degree

of Master of Science

DECLARATION

I hereby declare that this thesis has been composed by me, is a record of work carried out by me, and has not previously been presented for a Higher Degree.

The research was carried out in the Physical Laboratory of the United College of St Salvator and St Leonard in the University of St Andrews.

CERTIFICATE

I certify that Robert Alan Beveridge, B.Sc., has spent at least four terms as a research student in the Physical Laboratory of the United College of St Salvator and St Leonard, in the University of St Andrews, that he has fulfilled the conditions of Ordnance No.51 (St Andrews) and that he is qualified to submit the accompanying thesis in application for the Degree of Master of Science.

(Supervisor)

CAREER

I first matriculated in October, 1953 in the United College of St Salvator and St Leonard in the University of St Andrews and followed a course leading to graduation in June, 1957 with a Degree of Batchelor of Science with Honours in Natural Philosophy. In October, 1957 I commenced research in the Natural Philosophy Department in the same College on the work which is now presented as a thesis for the Degree of Master of Science.

TABLE OF CONTENTS

ILLUSTRATIONS

CHAPTER I

Introduction.

In a paramagnetic sample which is initially in thermal equilibrium with its surroundings, the energy states of the electron spin system are populated according to the Maxwell-Boltzmann distribution. If only two energy states of an electron spin system in a d.c. magnetic field are considered then the lower energy level is therefore more densely populated than the upper one, and the system can absorb energy from a radiation field of the correct frequency. Such an absorption of power disturbs the relative populations of the two energy levels of the spin system. The spin-lattice relaxation effect is one of the mechanisms whereby thermal equilibrium is restored, and can be characterised by a spin-lattice relaxation time.

The first work to be published on this subject was a theoretical study by Waller[1], the main interest being on the measurement of specific heats at low temperatures and the attainment of very low temperatures using the method of adiabatic demagnetisation. The earlier work of the Leiden school of research[2] showed that the understanding of these relaxation effects was far from complete, and many hypothetical mechanisms were suggested to reduce the discrepancies between the observed effects and theory, especially for measurements

made at liquid helium temperatures. Some of the early theories for the effects observed at low temperatures still give a fair understanding of the results of present day experiments on the measurement of spin-lattice relaxation times, but there are still many phenomena unexplained by modern theories.

With the development of very high frequency and microwave techniques new methods have been applied to the study of these problems. A further incentive to more detailed work and a further understanding of the mechanisms involved was the discovery and the application of the maser, an acronym for "Microwave Amplification by Stimulated Emission of Radiation". As a low noise amplifier the maser can be used to great effect as the first stage of amplification in observing and measuring signals with a very low signal to noise ratio such as occur in radio astronomy and long range radar systems. (3)(4) This device depends on the disturbance of the Boltzmann population of the energy states of a spin system by microwave radiation, and the use of the energy emitted in the return to thermal equilibrium. The efficiency of operation depends on the material which is being excited and the strength of the spin-lattice interaction, which determines the length of time the electronic populations will be in an emissive state.

Scope of Thesis.

In this thesis is reported the development of a 3 cm. paramagnetic resonance spectrometer to measure spin-lattice relaxation. This work was initiated as part of a programme of investigations in the field of electron spin resonance at the University of St Andrews and in particular to investigate specimens suitable for a two level solid-state maser. The method of measurement used in this work is the continuous wave saturation one where the intensity of the absorption of power from the incident microwave radiation is measured as a function of the incident power level.

Chapter 2 covers the essentials of the theory of spin-lattice relaxation effects and details of the specimens of neutron-irradiated diamond studied.

In Chapter 3 the construction and operation of the spectrometer to measure spin-lattice relaxation times at liquid helium temperatures is described in detail.

Chapter 4 is a report of the experimental results to date and some suggestions for improvement of technique and future experiments are also included.

CHAPTER II

General Theory of Paramagnetic Resonance and Relaxation.

The theory of paramagnetic relaxation effects has its foundations in a paper by Waller[1] and the experimental work at Leiden on high frequency and static susceptibility measurements. By these methods the effects of dilution of the number of paramagnetic centres could be studied, but the microwave resonant techniques developed after 1945 are better fitted for these studies. The first report of paramagnetic resonance was by Zavoisky[5], and the earlier work and theory is reviewed in a monograph by Gorter[2] and in a report by Cooke.[6] Other reviews of general paramagnetic resonance theory include references (7,8,9,10). This Chapter is devoted to a brief discussion of the paramagnetic resonance theory necessary for the description of mechanisms and methods of measuring the spin-lattice relaxation time in the samples studied.

2.1. Paramagnetic Resonance Theory.

Paramagnetism is usually associated with the presence of a permanent magnetic moment in atoms, molecules or ions which have a partly filled electron shell. Many examples of this occur naturally in the iron and rare earth groups of the periodic table, and in free radicals. One or more unpaired electrons may also arise due to certain types of imperfections

in a crystal, and these will also show paramagnetism.[11] Types which have been studied by electron spin resonance techniques include colour centres in alkali halides and defects produced by irradiation. It is the study of the second type of defect which has been the main work for this thesis, namely on neutron-irradiated diamond. In this case the irradiation breaks some of the strong co-valent bonds causing lattice damage. Thus atoms are knocked from their proper place in the lattice leaving interstitial atoms and vacancies, or groups of adjacent vacancies. Detailed discussion of this is left until Section 2.7.

In zero magnetic field, the magnetic moments associated with a system of free spins will be randomly orientated. On the application of a d.c. magnetic field, H, these magnetic moments can assume only two directions, either parallel or antiparallel to the direction of the applied field, corresponding to the magnetic spin quantum numbers of $\pm \frac{1}{2}$. The spins will now therefore fall into two different energy groups, with an energy difference of $g\beta H$ between the two energy levels, g being the spectroscopic splitting factor and β the Bohr magneton.

The distribution of the electron spins between these two states is given by the Maxwell-Boltzmann expression in which the ratio of the number in the upper state, N_1, to that in the

lower state, N_2, is given by

$$\frac{N_1}{N_2} = e^{-\frac{g\beta H}{kT}} \qquad (2.1)$$

where k is Boltzmann's constant and T is the absolute temperature of the spin system. If there are N_o free electron spins present in the sample, the difference in the populations of the two levels is given by

$$n = N_2 - N_1 = N_o \left(\frac{1 - e^{-\frac{g\beta H}{kT}}}{1 + e^{-\frac{g\beta H}{kT}}} \right) \qquad (2.2)$$

If now an alternating r.f. magnetic field is applied to the system of spins, as well as the d.c. magnetic field H, transitions will be induced between the two electronic energy levels, if the following resonance condition is satisfied

$$hf = g\beta H \qquad (2.3)$$

Thus a spin in the lower energy level can absorb one quantum of energy and jump into the upper state, and the reverse process may also occur with the emission of energy. If the distribution is given by equation (2.1) there are more electrons in the lower level, and a net absorption of energy will occur, the intensity of the absorption being proportional to the difference in the populations of the two levels (equation 2.2).

2.2. Paramagnetic Resonance at Microwave Frequencies.

The resonance condition states a direct proportionality between the d.c. magnetic field value, H, and the frequency of the radiation, f. The choice of operating frequency is usually a compromise of cost, sensitivity and ease of operation, but the best operating conditions are in the microwave frequency range with a d.c. magnetic field value between 1,000 and 15,000 gauss. These are the limits within which suitable microwave power sources and components, and adequate d.c. magnetic field homogeneity over the sample can be economically obtained for paramagnetic resonance work. Further consideration is given to this in Chapter 3.

The number of transitions induced between the two energy levels is proportional to the population differences in (2.2) and this can be increased by increasing H or decreasing T. The limits on the value of H and its dependence on frequency are discussed above. We consider now the effect of lowering the operating temperature by the use of liquified gases. By using the approximation $hf \ll kT$, which is valid in all cases when the temperature of the system is much greater than $0.45^{\circ}K$, the order of $\frac{hf}{k}$ in $^{\circ}K$.,

$$e^{-\frac{g\beta H}{kT}} = e^{-\frac{hf}{kT}} \doteq 1 - \frac{hf}{kT} \qquad (2.4)$$

and substituting this in equation 2.2 the change in population

for a decrease in temperature is worked out in Table 1. The frequency f is 9,375 Mc/S.

Table 1.

$T^{\circ}K$	290	83	20	4.2	1.2
Ratio of n at $T^{\circ}K$ to n at $290^{\circ}K$	1	3.5	14.5	59.5	235

(the approximation stated is not valid for temperatures below $20^{\circ}K$ and equation 2.2 was used below this temperature).

The ratio of populations at room temperature is 0.998 for 3 cm. wavelength. Thus, if we assume the conditions in the spectrometer remain the same at all temperatures, the figures in the Table 2.1 show the sensitivity will increase by a factor of 235 if the operating temperature is reduced from room temperature to that of pumped liquid helium. However, other factors dependent on temperature arise which affect the sensitivity, and these are discussed in Chapters 3 and 4.

2.3. Spin-Lattice and Spin-Spin Interaction.

The energy levels of the spin system are not perfectly sharp and thus the frequency of the absorbed or emitted radiation is not monochromatic but has a natural width due to the Heisenberg Uncertainty Principle. The spontaneous emission, however, is not sufficient to maintain the nett absorption of energy from the continuous microwave radiation, and some other mechanism must be present to allow the electrons in the upper

state to lose energy and drop back into the lower energy level. If this were not so then the larger number absorbing energy in the lower state would tend to equalise the populations, and no further absorption would occur.

One such effect is through the spin-orbit and orbit-lattice coupling of the electron. Although the actual proposed mechanism of this spin-lattice interaction is not fully understood (Section 2.5), this relaxation process whereby the energy of the spin system is being transferred to the lattice of the crystal can be characterised by a spin-lattice relaxation time, T_1. It is defined as the time in which an initial excess of energy given to the spins will fall to $\frac{1}{e}$ of its value, in the absence of any further applied radiation. A strong interaction therefore produces a short relaxation time, and a weak interaction produces a long relaxation time. This process is strongly temperature dependent as shown later.

The spin-spin interaction is a relaxation effect between the individual electron spins, and by this the whole spin system is brought into equilibrium. This means that energy absorbed locally in the spin system is spread over the whole system equalising the energy of all spins, and this is the justification for a unique spin "temperature" being ascribed to the system.

This interaction arises from the fact that an electron in a paramagnetic material is being acted on not only by the d.c. magnetic field, but also by the magnetic field due to

neighbouring electron spins each with a permanent dipole moment. These interactions between electron spins depend on the angle between the spins and the location of the spins with regard to each other. Each dipole is precessing about the d.c. magnetic field direction, and its components have an effect on neighbouring dipoles. This has the effect of producing a rotating field of the same frequency as the frequency of precession and tending to change the direction of the neighbouring dipole. Thus there is a broadening of energy levels and a tendency to reduce the lifetime of an electron in a given state. This has been studied in detail by Van Vleck[12], and Pryce and Stevens[13], and the mechanism is normally described by the spin-spin relaxation time, T_2. This is usually short, of the order of a microsecond, and is temperature independent. The line width is usually written as

$$\Delta\omega = \frac{1}{T_1} + \frac{1}{T_2} \qquad (2.5)$$

Thus the line width is determined entirely by the spin-spin interaction if $T_1 >> T_2$, and

$$\Delta\omega \doteq \frac{1}{T_2} \quad \text{or} \quad g(\omega_o)_{max.} = \frac{T_2}{\pi} \qquad (2.6)$$

where $g(\omega-\omega_o)$ is the normalised line shape function and has a maximum at ω_o.

2.4. Saturation Effects.

Saturation occurs when the absorption of radiation by the paramagnetic molecule is not linearly dependent upon the power level of the applied radiation. As the density of the incident radiation is raised slowly the number of spin transitions to the excited state will increase until such time as the relaxation mechanisms can no longer maintain the original thermal equilibrium of the spin system. Then the population difference between the states decreases and the linear dependence of the absorption on the density of the incident radiation no longer holds. Complete saturation occurs when the two population levels are equal and then the paramagnetic system may be said to be transparent to the incident radiation.

Following the analysis of Bloembergen, Purcell and Pound[5], and of Portis[14], the deviations of a two-level spin system from equilibrium with the lattice due to the incident radiation is given by

$$\frac{dn}{dt} = \left(\frac{dn}{dt}\right)_{r.f.} + \left(\frac{dn}{dt}\right)_{s.l.} \qquad (2.7)$$

where $n = N_2 - N_1$, and $\left(\frac{dn}{dt}\right)_{r.f.}$ and $\left(\frac{dn}{dt}\right)_{s.l.}$ give the rate of change of the difference in populations from the interaction with the radiation field and spin-lattice interaction respectively. The rate of change of population due to the

interaction with the radiation field of frequency ω is

$$\left(\frac{dn}{dt}\right)_{r.f.} = -\frac{1}{4}\pi\gamma^2 H_1^2 g(\omega-\omega_o)n$$

where γ is the gyromagnetic ratio of the electron, and H_1 is the maximum amplitude of the r.f. field,

$$\left(\frac{dn}{dt}\right)_{s.l.} = \frac{n_o - n}{T_1} \qquad (2.9)$$

This describes the tendency of the spin system to come to thermal equilibrium with the lattice in the absence of an r.f. field, and n_o is the difference in populations at thermal equilibrium.

If the microwave power is varying slowly compared to T_1, the rate of change of the populations will be close to zero and this quasi-steady state may be described by

$$n = n_o\left[1 + \frac{1}{4}\pi\gamma^2 H_1^2 T_1 g(\omega-\omega_o)\right]^{-1} \qquad (2.10)$$

The rate at which energy is absorbed from the radiation field is

$$P_a = -\frac{1}{2}\hbar\omega\left(\frac{dn}{dt}\right)_{r.f.}$$

$$= \frac{1}{2}\omega\left\{\frac{1}{2}\omega_o\left(\frac{\gamma^2\hbar n_o}{2\omega_o}\right)\ \frac{\pi g(\omega-\omega_o)}{1 + \frac{1}{4}\pi\gamma^2 H_1^2 T_1 g(\omega-\omega_o)}\right\} H_1^2 \qquad (2.11)$$

As is shown by Bloch[15] (a treatment which was originally applied to nuclear magnetic resonance effects[16]), the magnetic properties can be described in terms of the susceptibility. In a high frequency magnetic field, the magnetisation of a specimen does not follow the high frequency variation of the magnetic field instantaneously, and a phase lag occurs. The susceptibility is written in the complex form

$$\chi = \chi' - i\chi'' \qquad (2.12)$$

where χ' and χ'' are related to dispersion and absorption of power from the high frequency field. The total energy absorbed by the spin system is

$$P_a = \frac{1}{2}\omega\chi''H_1^2 \qquad (2.13)$$

In a steady magnetic field the susceptibility has a static value

$$\chi_o = \frac{\hbar\gamma^2}{4KT}n_o = \frac{\gamma^2\hbar n_o}{2\omega_o} \qquad (2.14)$$

From (2.11), (2.13) and (2.14) we get

$$\chi''(\omega) = \frac{1}{2}\chi_o\omega_o \frac{\pi g(\omega-\omega_o)}{1 + \frac{1}{4}\pi\gamma^2H_1^2T_1g(\omega-\omega_o)} \qquad (2.15)$$

In equation 2.6, T_2 is defined at the centre of the absorption line as

$$g(0) = {}^{T_2}/_{\pi}$$

Then

$$\chi''(\omega_0) = \frac{1}{2}\chi_0\omega_0 T_2 \frac{1}{1 + \frac{1}{4}\gamma^2 H_1^2 T_1 T_2} \qquad (2.16)$$

The last term in this equation is called the "saturation factor" S.

$$S = (1 + \tfrac{1}{4}\gamma^2 H_1^2 T_1 T_2)^{-1} \qquad (2.17)$$

and by comparison with equation (2.10) it is seen that

$$S = \frac{n}{n_0}$$

i.e. the ratio of the difference of population with saturation to the difference in population when the spin system is in thermal equilibrium with the lattice.

Equation (2.17) implies that the absorption of power will be lower the larger the value of T_1 and will fall off with increase in the density of the microwave irradiation. This decrease occurs first in the centre of the line and will affect the wings of the absorption curve only on further increase of power i.e. saturation broadening. The above analysis applies only when the broadening is of the homogeneous type, i.e. arises from the dipolar interaction between the spins (Section 2.3) or from the interaction with the radiation field. Thus the energy absorbed from the microwave field is distributed to all the spins and thermal equilibrium of the spin system is maintained through resonance.

2.5. Proposed Mechanisms for Spin-Lattice Relaxation Effects.

In the original paper by Waller[1] two relaxation processes were postulated: a direct process in which a spin absorbs or emits a single phonon (or a quantum of lattice vibrations) at the frequency of the spin transition, and an indirect or Raman process in which one phonon is absorbed and another is emitted at a frequency differing from the frequency of absorbed phonon by an amount equal to the frequency of the spin transition. This proposition was considered in (17) and (18) but the spin-lattice relaxation times predicted were too long. Kronig[19] showed that the spin-orbit coupling has the effect of transmitting the lattice vibrations to the spins and thereby orientating them with respect to the external magnetic field, and by this means he arrived at relaxation times of the correct order of magnitude. The Raman process is dominant at temperatures down to the liquid helium range, being proportional to T^7, and only at very low temperatures does the direct process effect the relaxation, this being proportional to T.

However, these theories did not explain the experimental results[20][21] worked out on the basis of the thermodynamical model of Casimir and du Pré[22] and of Debye[23]. Experimental work continued at Leiden and Oxford and other attempts to explain the differences between the experimental results and the theoretical predictions were made by Van Vleck[24], Temperley[25] and Bijl[26]. A review of these developments is given in references (2) and (6).

With the advent of microwave resonant techniques and the solid-state maser many other refinements of the above theory have been proposed, including the consideration of the mean free path of the lattice phonon with the possibility of phonon imprisonment[27][28]. This could produce a phonon-bath bottleneck in the spin-lattice relaxation[29][30]. The work of Giordmaine et al.[31] on lattice-bath bottlenecks and the possible spread of phonons on "speaking terms" with spins, which allows uniform saturation of the crystal[32], have all been questioned as regards three-level maser operation. Cross-relaxation has been introduced by Bloembergen[33] in which energy is transferred amongst the various lines of a multilevel system by means of multiple spin transitions. This can effect the establishment of thermal equilibrium of the spin system and provides an explanation ~~for~~ of some ~~of~~ effects reported in (31), (32).

There is still no completely satisfactory explanation of spin-lattice relaxation, and none of the proposed theories to date explain the dependence on temperature and the dilution of the paramagnetic centres. Thus the main experimental approach has been to study the effects of temperature and concentration on the relaxation time. A recent survey of the possible mechanisms and their faults has been given by Van Vleck[34].

2.6. Experimental Methods.

a) Measurement of the absorption of power at radio frequencies by the paramagnetic specimen was the first method to be used to detect spin-lattice relaxation effects[2]. The specimen is placed in an alternating magnetic field of amplitude H_1 and the heat generated in the specimen gives a measure of the imaginary component of the susceptibility.

Alternatively, audio frequencies may be used, the changes in the mutual inductance of two coils placed round the specimen being a measure of the magnitude of the real and imaginary part of the susceptibility. The most convenient way of doing this is to use an a.c. bridge and Bijl[26] reports experiments using this method.

b) There are three methods of measuring the spin-lattice relaxation time using microwave resonant techniques.

The first to be described is the one used for experiments to be reported in this thesis: the "continuous wave saturation method" which was originally developed in nuclear magnetic resonance[5]. Reports of the use of this method for paramagnetic experiments are found in references (14), (35), (36) and (37). It consists of measuring the magnitude of the resonance absorption as a function of the microwave power incident on the sample. This is done by including one calibrated attenuator in the input power arm to vary the level of the incident radiation, and a second calibrated attenuator in the reflected signal arm of the microwave bridge is adjusted

until the same level of power is detected for each setting of the first attenuator. This is equivalent to measuring the change in the height of the absorption signal for a change in input power.

Inherent in this method are the assumptions that the effect of the spin-lattice interaction is to relax the spins to their equilibrium state in time T_1, and that the spins interact strongly with each other so that energy absorbed at one frequency is quickly transferred to all the spins i.e. $T_2 \ll T_1$. It also assumes that the complex susceptibility is proportional to the difference in the population of adjacent electronic energy level. This means that the spin system behaves as if it were at equilibrium at a spin temperature higher than the lattice temperature.

The other methods used rely on observation of the absorption as a function of time after the spin populations have been disturbed by microwave power. In the "saturation-recovery" method the recovery of the absorption is monitored as a function of time after a pulse of power of sufficient intensity and duration to saturate the absorption is applied, the magnetic field being held constant at the value corresponding to maximum absorption[38][39]. The "inversion-recovery" method uses adiabatic fast passage[15] of the magnetic field through the resonance to invert the spin populations and observes the recovery to equilibrium of the whole line as a function of time.

This is a method similar to the techniques used in maser experiments, and differs from the saturation recovery method in that the incident power is being applied to the whole absorption line. It is claimed that this method will show any phonon-imprisonment or bottlenecks as a change in the slope of the recovery to thermal equilibrium.

2.7. Paramagnetic Resonance in Neutron-Irradiated Diamond.

Earlier work by Griffiths et al.[40] suggests that neutron irradiated diamond is a suitable paramagnetic crystal for the study of spin-lattice relaxation effects. Dugdale[41] observed the colouration of diamond due to neutron bombardment. On heat treatment to 1000°C this dark green colouration gradually decreased in intensity to an ultimate pale yellow, and he suggested the colouration is due to the formation of Frenkel defects (by the neutron bombardment), i.e. vacant lattice sites and interstitial atoms.

The first report of paramagnetic resonance studies of neutron-irradiated diamond is by Griffiths et al.[40a] with measurements taken from 20°K to 290°K at a wavelength of 1.2 cm. and 3.1 cm. They report many closely spaced lines classified as follows:-

a) A single absorption line, much more intense than all the others with a g-value of 2.0028 (for a free electron g = 2.0023). Both the intensity and line width increase with the irradiation dose, as does the colouration, but they decrease rapidly if the

diamond is heated. In the table below ΔH is the line width.

Irradiation time	10 hours	120 hours	180 hours
Colour	pale green	dark green	black
ΔH at 290°K	20 gauss	47 gauss	70 gauss
ΔH at 20°K	15 gauss	21 gauss	26 gauss

(the integrated neutron flux for 1800 hour exposure was 9×10^{18} neutrons/cm^2).

b) An anisotropic spectrum of twelve lines with intensity of order 100 times smaller than that of the central line. The intensity and the line width are independent of temperature, and the investigators suggest this spectrum may be explained as arising from paramagnetic units with electronic spin S = 1, the spin levels being separated into a doublet and singlet (separation D = 0.010 $cm.^{-1}$) by a crystalline electric field of nearly axial symmetry. This axis is parallel to one of the six edges of the fundamental carbon tetrahedron of the diamond lattice, so that there are six differently oriented units present each giving two lines in the spectrum. The positions of these can be found from the spin Hamiltonian

$$\mathcal{H} = \beta H.g.S + DS_z^2$$

where the mean g-value is g = 2.0027, $\frac{g_\perp}{g_\parallel} = 1.0035$ and $|D| = 0.010$.

c) Many other smaller lines whose intensity and position vary from sample to sample.

From these results it is concluded that the absorption spectrum is due to lattice defects and the intensity is qualitatively proportional to the duration of irradiation. The spectrum is in no way connected with impurity atoms except possibly type c) lines. The intensities and line width suggest the centres occur in clusters.

O'Brien and Pryce[42] give a theory which suggests that the main absorption peak is due in part to isolated vacancies. One isolated vacancy has four carbon atoms as its nearest neighbours each with an unpaired electron. The most probable ground state of this system is one in which all the spins are parallel ($S = 2$) but splitting is negligible due to the high state of symmetry. The resultant absorption is a single isotropic line with the free spin g-value. The investigators give no further explanation of the type b) lines except to observe that the diamond structure is very open and the natural interstitial position for an atom is the same distance from its nearest neighbours as are ordinary carbon atoms in diamond. The splitting and g-value can be related to the ^3P state of carbon. A further refinement is that two interstitial carbon atoms may join to form a C_2 molecule with $S = 1$. Although the detailed theory is not clear many effects can be explained by the over-simplified model in which the type a) line arises from single vacancies or interstitials, or both, and the type b) lines arise from C_2 molecules.

The effect of heat treatment then is that the interstitials

drop back to fill the nearest vacancies with a corresponding decrease in the main line absorption, and only the spectrum due to the C_2 molecules remains. This is what is observed and can also be fitted to the optical absorption work[43].

2.8. Neutron-Irradiated Diamond Specimens.

The diamonds available for investigation were kindly supplied by the Physics Research Laboratory, University of Reading. The six specimens obtained were irradiated in the B.E.P.O. reactor but the exact details of the irradiation dose are not known. The data listed in the following table is based on a comparison of the optical absorption spectra of other neutron irradiated diamonds at the University of Reading.

Specimen	Colour	n_o dose at pile factor 6	Weight (cts.)
D 23	clear	1 hour	0.52
D 24	clear	3	0.41
D 25	pale green	10	0.17
D 26	pale green	30	0.22
D 27	dark green	120	0.38
D 29	black	1000	0.35

(Pile factor 1 is a neutron flux of 10^{11} neutrons/cm.^{2}/secs.)

The crystals are irregular slices approximately 0.5 mm. thick and 4 mm. in diameter. From the above it is estimated that specimens D 27 and D 29 were exposed to an integrated neutron flux of approximately 2.5×10^{16} and 2×10^{17} cm^2 respectively.

CHAPTER III

Description of the Apparatus.

3.1. Introduction.

This chapter is devoted to the description of the design and construction of a 3 cm. microwave spectrometer to operate at liquid helium temperatures. In choosing the operating frequency several factors have to be considered, namely the optimum sensitivity required, the cost and availability of microwave components and a d.c. magnet, and the ease of operation. The final choice is a compromise of these factors and they are now treated in more detail.

From cost considerations, it is cheaper to use 3 cm. microwave equipment than 8 mm. components, because the components for the shorter wavelength must be manufactured to stricter tolerences. The requirement for a higher stable d.c. magnetic field for work in the higher frequency range also adds greatly to the cost.

Besides the actual value of the d.c. magnetic field and the high homogeneity required, the distance between the pole faces of the magnet is one of the main consideration in the design and size of the resonant cavity. Since cryogenic techniques have also to be used, it is simpler if the cavity is of the reflection type with the specimen mounted on the bottom in a region of maximum r.f. magnetic field. If the cavity was resonant at the higher frequencies, i.e. shorter length, the

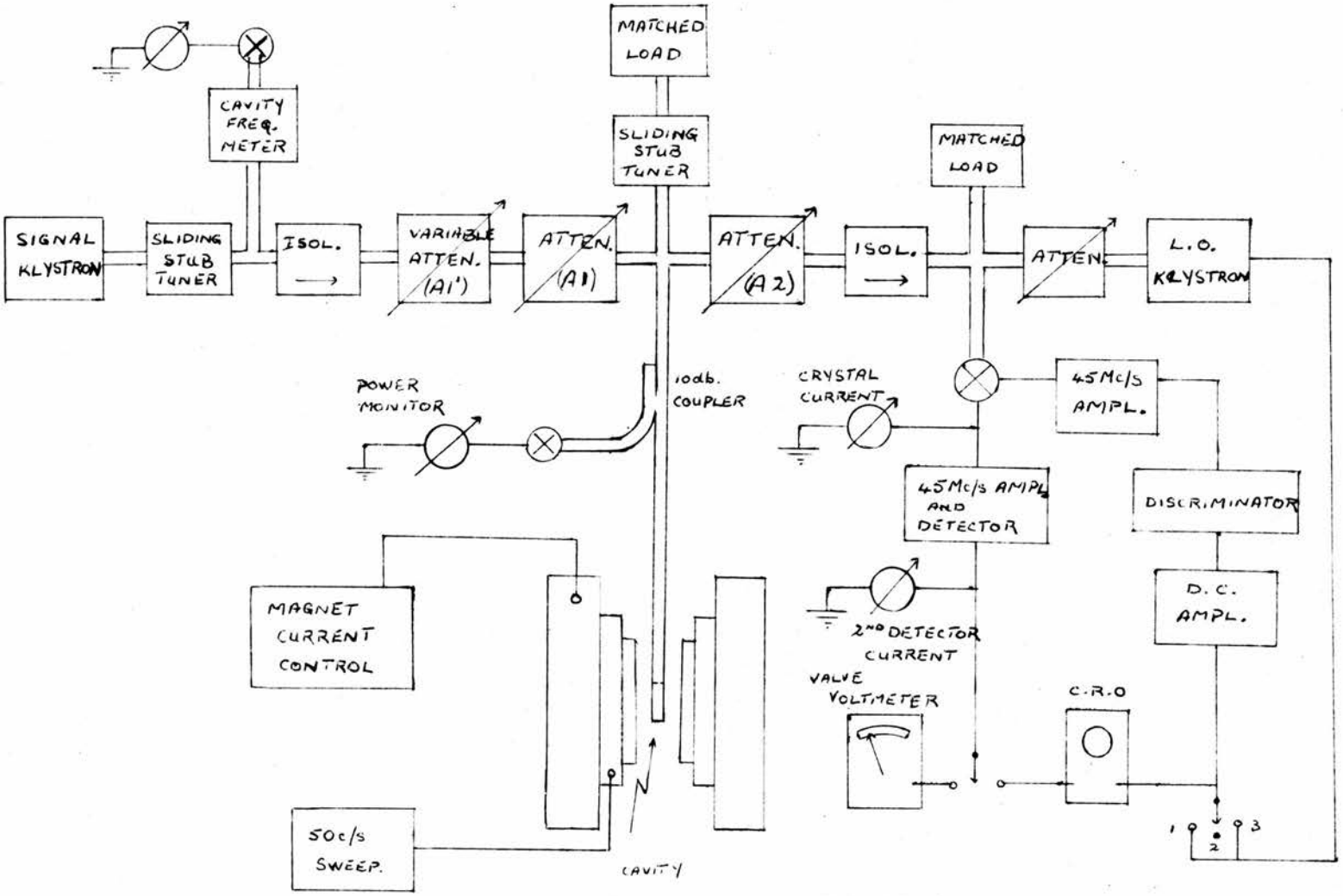

Fig. 1. Block Diagram of Apparatus.

specimens would not be confined to the area of high r.f. magnetic field, and thus the Q-value of the cavity would be lowered with a corresponding decrease in the sensitivity. Feher[44] considers the "minimum number of detectable spins per unit volume" as a suitable measure of the sensitivity of a spectrometer.

A block diagram of the apparatus is shown in Figure 1. The two accurately calibrated attenuators, A1 and A2, are used respectively to vary the microwave power incident on the cavity by a known amount, and to make a suitable adjustment for this change in the measured reflected signal. By tracking A2 against A1, with a suitable conversion of units, an accurate saturation curve can be plotted.

In this method of measuring the spin lattice relaxation time a wide range of power output from the signal source is necessary. The choice of klystrons satisfying this requirement is wider at 3 cm. than 8 mm. operating wavelength. Detecting systems are generally more noisy at the higher frequency, and all these considerations of cost, lack of power, and noisy detection counterbalance any theoretical gain in sensitivity due to the use of a higher frequency spectrometer.

It is also shown in the block diagram that a balanced magic tee is used to decouple the incident and reflected microwave signals, and to facilitate the detection of the absorption signal as a small power change over a normal zero power level. To give better sensitivity superheterodyne detection is used,

as the noise generated in semiconductor crystals at low frequencies is appreciable. This becomes negligible at frequencies of the order of tens of megacycles or higher[44].

The reflected signal from the cavity is mixed at a second magic tee with another microwave signal from a local oscillator operating at a frequency removed from the signal klystron by the intermediate frequency. In this case the I.F. is 45 Mc/s, and the detecting crystal output is at this frequency. Since the voltage produced at such a crystal is proportional to the microwave power incident on it for low signal voltages, i.e. linear detection, the mean level of this detected signal is of the order of the local oscillator power. The maximum voltage change transmitted to the detector due to a resonance absorption occurs when the bridge magic tee is correctly matched. Thus a matched load is placed in the arm of the tee opposite to the cavity arm. However if the V.S.W.R. of the cavity arm is very close to unity, i.e. the cavity is close to critical coupling, the absorption signal from the cavity might change the coupling condition and distort the resonance line due to the change in sign from an overcoupled to an undercoupled state. Control of the matching of the bridge is arranged by including a sliding stub tuner in one of the matched arms, and tuning the system to make it sensitive to the imaginary part of the susceptibility only.

Details of the microwave components and the associated electronics are discussed in the rest of this chapter.

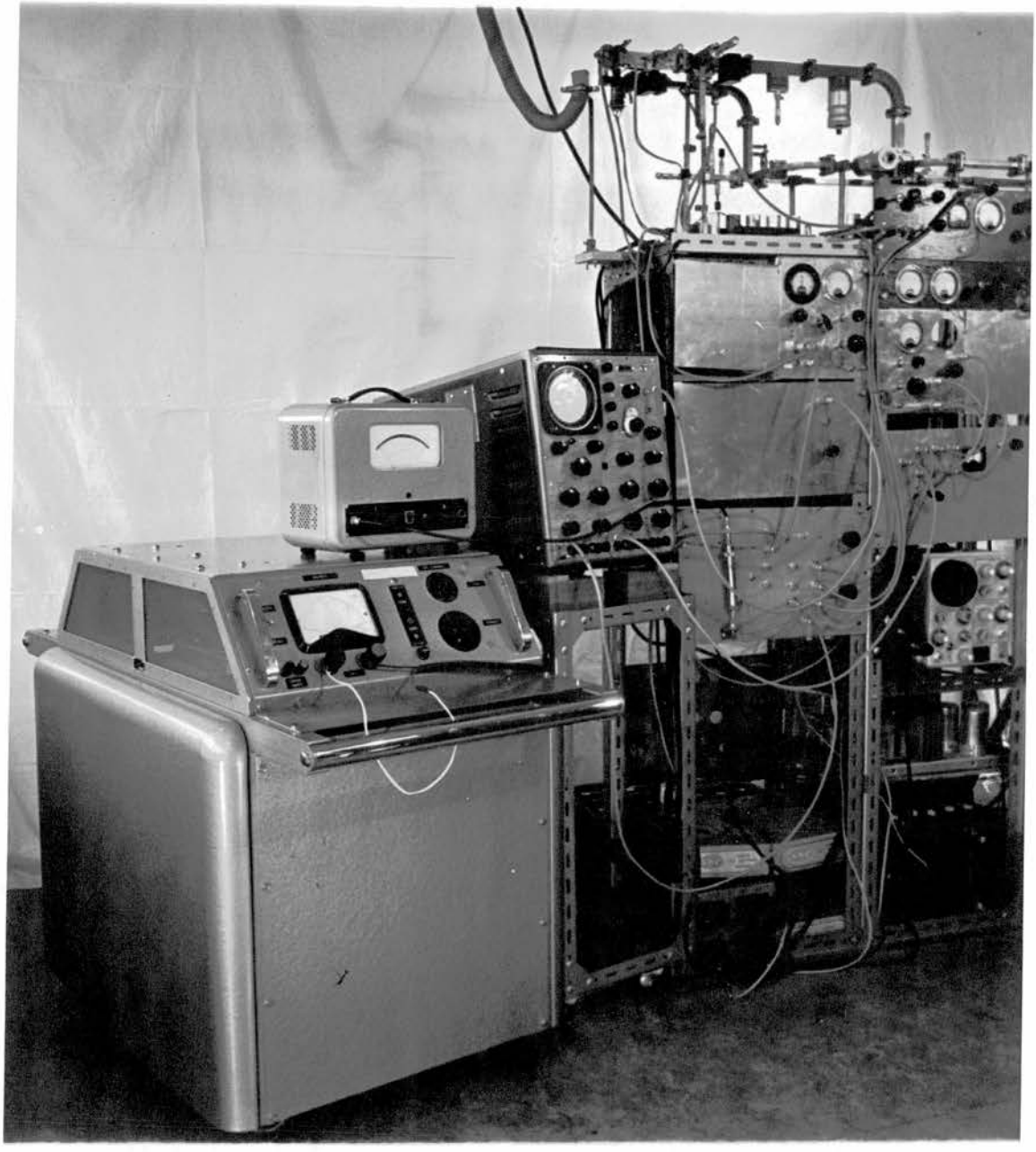

Fig. 2. Microwave Bridge and Electronics.

3.2. Microwave Circuitry.

From the block diagram of the microwave and electronic components, Figure 1, and the photographs of the apparatus, Figures 2, 6, the design of the spectrometer and its practical arrangement can be seen. All commercially bought components are listed in the Appendix; the other waveguide units were fabricated in the laboratory workshops from American size waveguide tubing No.16 with inner dimensions 0.900 in. x 0.400 in.

3.2.a) Input Circuit.

Signal Klystron.

A Varian X-13 reflex klystron was chosen as a suitable high power output stable source. The mechanical tuning with a micrometer head gives a wide frequency range from 8.2kMc/s to 12.4kMc/s. Depending on the matching of the load, the power output from this source can vary from 200 mw. to 550 mw. The electronic tuning range is governed by the possible voltage variation of the reflector voltage. The supply and control circuits, together with the safety devices are shown in Figure 3.

The reflector potential is obtained from a stack of 120v. dry batteries, thereby ensuring there is no unwanted frequency modulation in the power output due to ripple in this voltage supply. To operate the X.13 Klystron in the $3\frac{3}{4}$ mode a reflector voltage of about -580v. with respect to

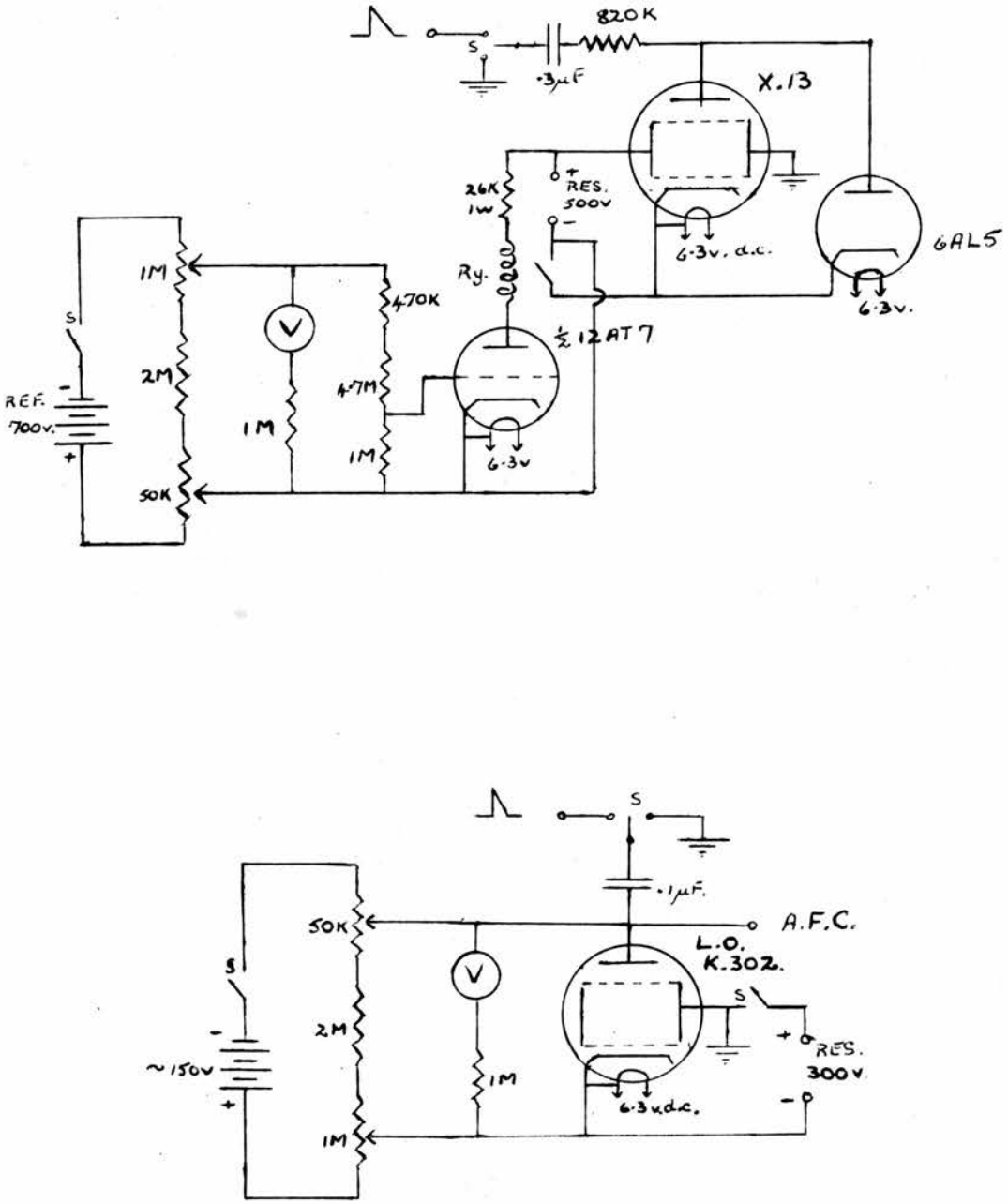

Fig. 3. Circuit Connections for Klystrons.

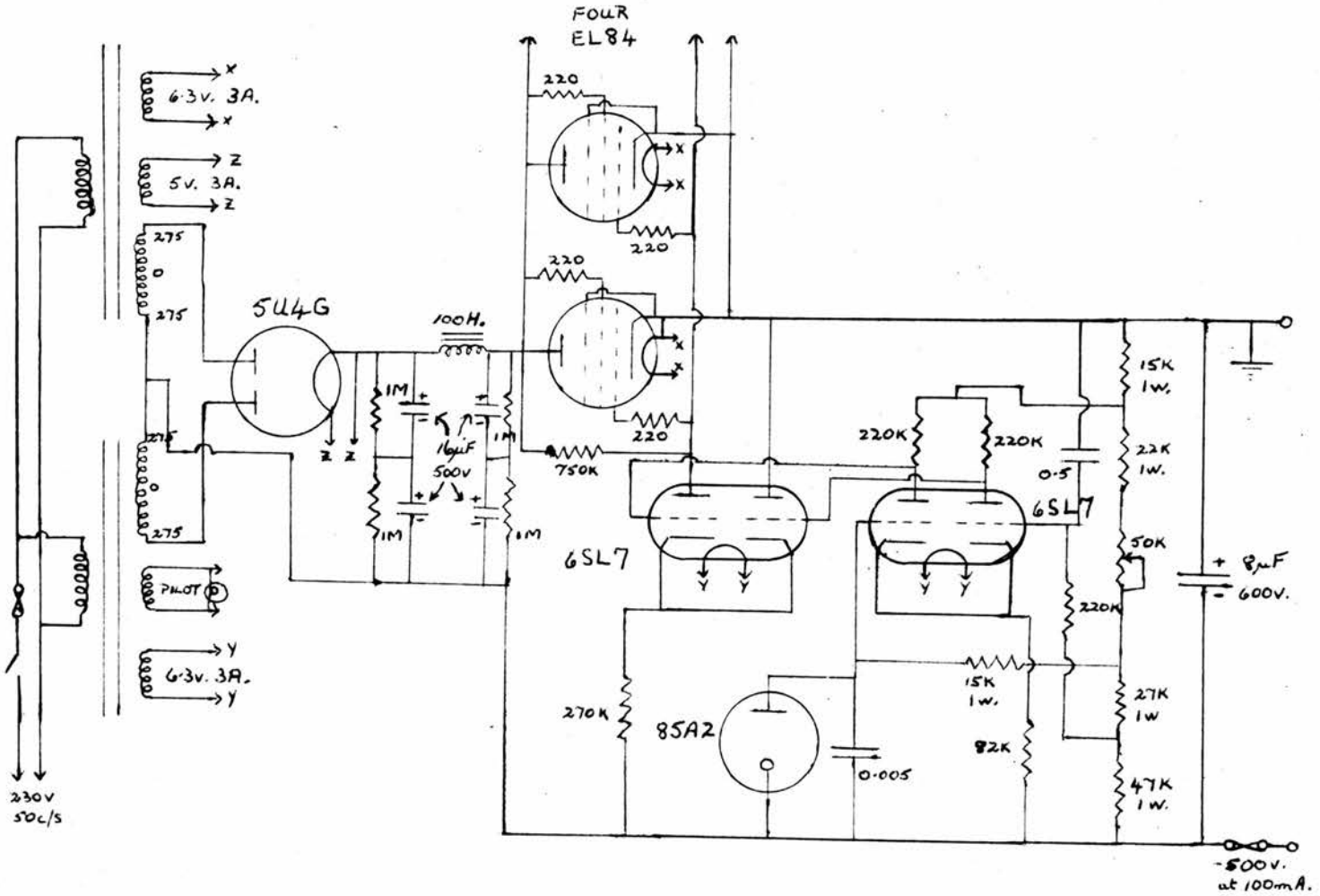

Fig. 4. X-13 Klystron Power Supply.

the cathode is required, but variation of this voltage over the full range of this mode from 500v. to 670v. is made available by including a course and fine variable resistance system. The current drain from these batteries is small depending only on the resistance of the control circuit. Also shown in the Figure is a 6AL5 protective diode to ensure that the reflector will not become positive with respect to the cathode, as such an occurence can damage the klystron. In addition a mechanical relay is included in series with the output of the resonator power supply to cut off this supply should the reflector voltage fail.

A further safeguard against the introduction of any undesirable 50 c/s frequency modulation on the microwave output is the use of a 6.3 volt Ni-Fe battery for the klystron heater supply. A battery charger was built into the apparatus so that the battery could be charged in situ.

The circuit of the -500v. resonator power supply is shown in Figure 4 and a full discussion of the design of this is left until the section on power supplies (3.8a)).

When this klystron is being operated on the $3\frac{3}{4}$ mode forced-air cooling must be supplied. The requirement of 30 cubic feet per minute was met by installing a large blower in an adjoining building to the laboratory and running a $2\frac{1}{2}$ in. diameter pipe from this to all points requiring forced-air cooling.

Sliding Stub Tuner.

As the power output of the signal klystron depends on the load presented to it by the microwave line, a sliding stub tuner is included. This consists of a variable capacitance probe whose position and depth can be controlled to close limits. Amplitude variation is effected by a micrometer screw-head operating against a spring loaded plunger which protrudes into the waveguide mounted on a moveable carriage. The position of this can be set by means of a vernier scale, or finely adjusted by a screw mechanism. Thus, by adjustment of the depth of insertion of the probe and the lateral position along the waveguide, an optimum load can be achieved to give any desired output from 200 mw. into a matched load to a maximum of 550 mw.

Cavity Frequency Meter.

The cavity frequency meter used is a transmission cavity type operating on the TE 112 mode. Tuning is controlled by a micrometer head moving a plain disc to change the length of the cavity, the range of tuning being 8,800Mc/s to 10,000Mc/s. The use of this with a crystal mount gives a measure of the frequency of the microwave signal to an accuracy of 1 part in 10^4, by tuning for maximum crystal current.

Besides this use, the cavity also serves to give a slight degree of frequency stability, since any drift in frequency from the frequency to which the wavemeters is tuned would produce a reflected signal. This pulls the klystron

back to the resonance frequency and acts as a rough but fairly effective form of stabilisation provided the Q-value of the wavemeter cavity is high enough.

Other uses of this meter are that it gives a measure of output power of the signal klystron and indicates any large drifts in the klystron frequency. It also provides a means of measuring approximately the Q-value of the resonant cavity.

Isolator.

Any further frequency pulling by the load presented by the microwave system to the signal klystron is avoided by using a ferrite isolator between the component previously described and the first of the calibrated attenuators. This isolator has a reverse attenuation of 20db. at an operating frequency of 9,375 Mc/s.

Attenuators.

Two variable attenuators are included in this arm, one of which is calibrated in steps of 1db. up to 40db., and the other is an accurately calibrated one with a large micrometer head, hereafter referred to as A1. Settings of this micrometer head can be read to an accuracy of 0.002 mm., which is equivalent to an accuracy of better than 0.005db. in the attenuation. However the sensitivity of the spectrometer to power level changes reduces this accuracy to 0.01db., and the accuracy of the calibration charts is not known. This attenuator gives a direct measure of changes of power incident on the cavity system.

Magic Tee.

This tee is the centre of the microwave bridge separating the incident and reflected microwave power paths from the cavity. Originally a tee fabricated in the laboratory workshop was used but latterly this was replaced by a Philip's Hybrid Tee milled from two blocks of metal which are accurately pinned together. The decoupling between the input and output arms (E- and H-arms) under correct matching conditions is better than 40db. The original tees made in the laboratory were supplied with tuning screws in the E- and H-arms at a sufficient distance from the junction to avoid any asymmetry and at a distance of $\frac{3}{8}\lambda_g$ apart[45]. By means of these the V.S.W.R. could be reduced to a minimum and the decoupling to a maximum when the components were set up on a test bench.

3.2.b) The Cavity Arm.

The components included in the cavity arm and the design of the entrant waveguide will be treated later (Section 3.4.c), where full consideration will be given to cryogenic requirements It is sufficient here to state that changes in the load presented to the magic tee are critical and may be compensated for by the inclusion of a sliding stub tuner in the arm of the bridge opposite to the cavity arm. This can effectively change the matching condition of the cavity giving some control of the amplitude and phase balance of the bridge. It can be seen from

the visual display on an oscilloscope of a paramagnetic absorption signal by a wide 50 c/s magnetic field sweep modulation that this sliding stub tuner position can be used to control whether the reflected signal is a function of the real part or the imaginary part of the susceptibility.

A power monitor was inserted in this arm by means of a 10db. directional coupler, and a crystal mount. The crystal current is a measure of the power incident on the cavity, but no absolute power measurements can be taken from this.

3.2.c) Detecting System.

The reflected signal from the cavity is subject to further attenuation in arm 4 of the brdige magic tee. This precision attenuator A2 is the same type as that described as A1 in the signal klystron arm, and the accuracy of setting is of the same order of magnitude (better than 0.005db for any setting depending on the sensitivity of the spectrometer to power level changes). This attenuator gives a measure of the reflected power from the cavity and any change in the incident power by varying attenuator A1 gives a corresponding change in the reflected power, which can be compensated for by a change in the attenuation A2. The detailed description of the use of these attenuator settings is given in Section 4.3.

Local Oscillator.

As indicated in Section 3.1 superheterodyne detection is used. An English Electric K.302 klystron serves as a

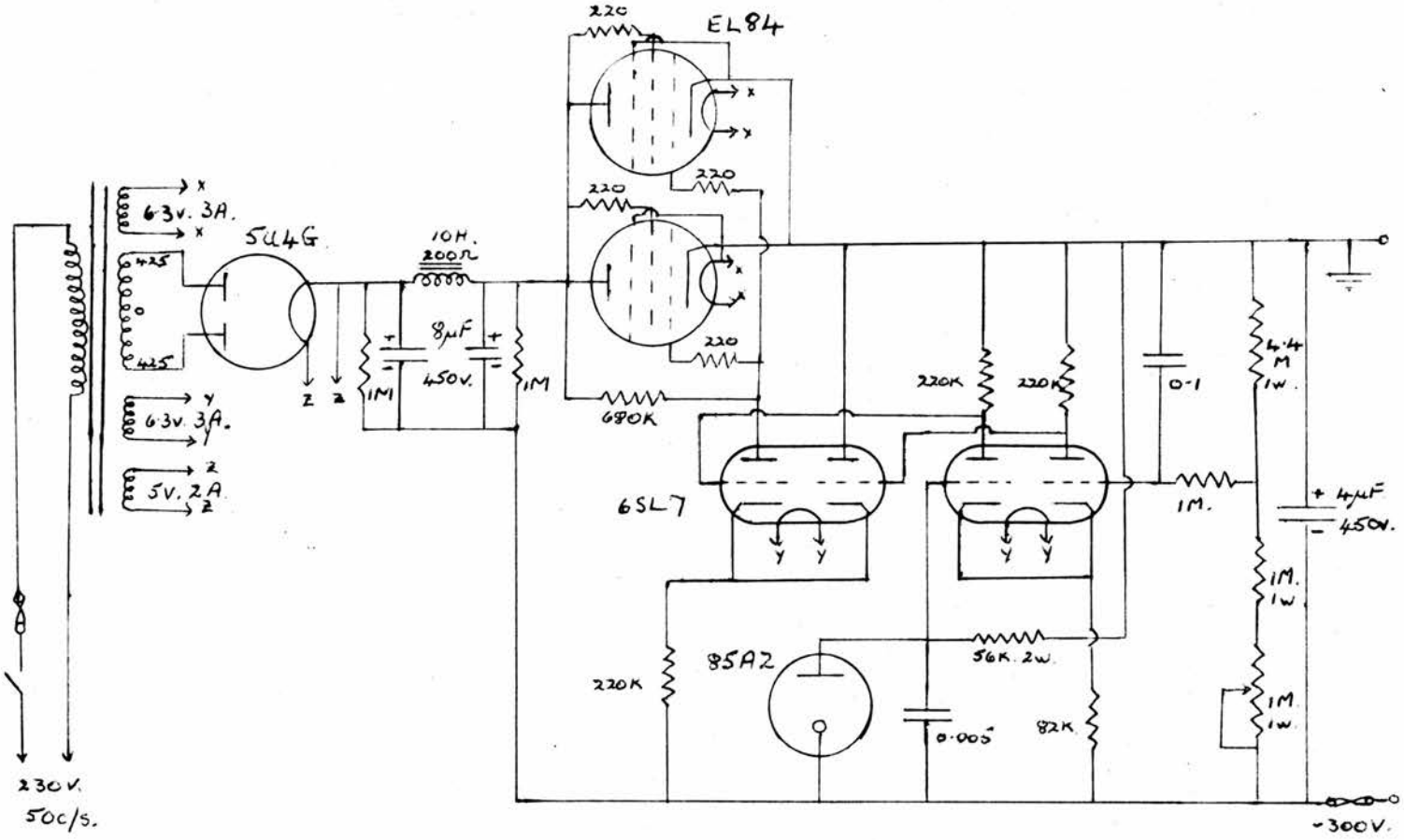

Fig. 5. L.O. Klystron Power Supply.

suitable local oscillator. Operating with a load V.S.W.R. close to unity this klystron has a power output of 30 mw., and requires no forced air cooling. A micrometer screw head gives a very easy and accurate mechanical tuning of the microwave output. The electronic tuning range is 30 Mc/s and the reflector voltave control circuit shown in Figure 3 is similar to that of the signal klystron. No safety devices were included. As for the signal klystron the reflector potential is taken from a stack of 120v. dry cells, and the heater is run from a 6.3v. Ni-Fe battery, both systems being used to avoid any unwanted ripple on the output microwave signal. The resonator power is supplied by the -350v. power unit shown in Figure 5. Prior to the purchase of this klystron a 723A/B reflex klystron was used as a local oscillator, but the new klystron gives improved frequency stability, a necessary condition if there is to be no I.F. drift.

Attenuator.

A variable attenuator is inserted between the local oscillator klystron and the mixing magic tee to control the level of power detected in the semiconductor crystal. A 30db. variation in power is obtained by moving the attenuator vane across the waveguide, the movement being governed by an external screw set against a millimeter scale.

Magic Tee.

The magic tee used to mix the reflected signal from the cavity and the local oscillator power is of the post and iris type, being fabricated in the laboratory workshops from standard waveguide tubing. The dimensions were taken from those given in volumes of the Radiation Laboratory Series[46][47]. To facilitate adjustment of the isolation properties and V.S.W.R. under matched conditions tuning screws are included in the E- and H-arms of this tee. Two capacitiv screws placed $\frac{3}{8}\lambda_g$ apart are sufficient to tune out most unwanted reflections, but these screws had to be sufficiently far away from the junction of the arms of the tee to avoid any asymmetry due to their presence. The other two arms of the tee are terminated by a matched load and crystal detector both with a V.S.W.R. close of unity.

Isolator.

To avoid any possible leakage of local oscillator power into the cavity arm an isolator, similar to the one in the signal klystron arm, is included in the section of the microwave bridge between the two magic tees, i.e. next to the calibrated attenuator A2. This presents 20db. reverse attenuation to any unwanted power.

Reflectionless Load.

The reflectionless loads were fabricated in the laboratory from tapered sections of soft pine wood. These fish-tail loads were inserted into a length of waveguide and an optimium position of the load could be found to give a minimum V.S.W.R.

Crystal Mount.

The original crystal mounts used are modelled on a type described in reference (48) and were manufactured in the workshops. These are furnished with two $\frac{3}{8}\lambda_g$ capacitive tuning screws and a variable shorting plunger, and designed to take a B.T.H. CS3-B detecting crystal. Latterly, the detecting unit was replaced by a custom built Philips adjustable crystal holder. This incorporates the same features as the original mounts, but has easier adjustment for a good V.S.W.R. i.e. less than 1.05 at the operating frequency. The semiconducting crystal used in this mount is a 1N23 crystal (or a B.T.H. CS3-A).

3.3. Alignment of Matched Loads, Crystal Mounts and Magic Tees using Test Bench.

Using a 723A/B klystron tuned to a frequency close to 9375 Mc/s. each of the above components from the spectrometer were coupled in turn to the test line and adjusted for a minimum voltage standing wave ratio. An attenuator and cavity wavemeter were included in the test bench to adjust the power and to monitor the frequency.

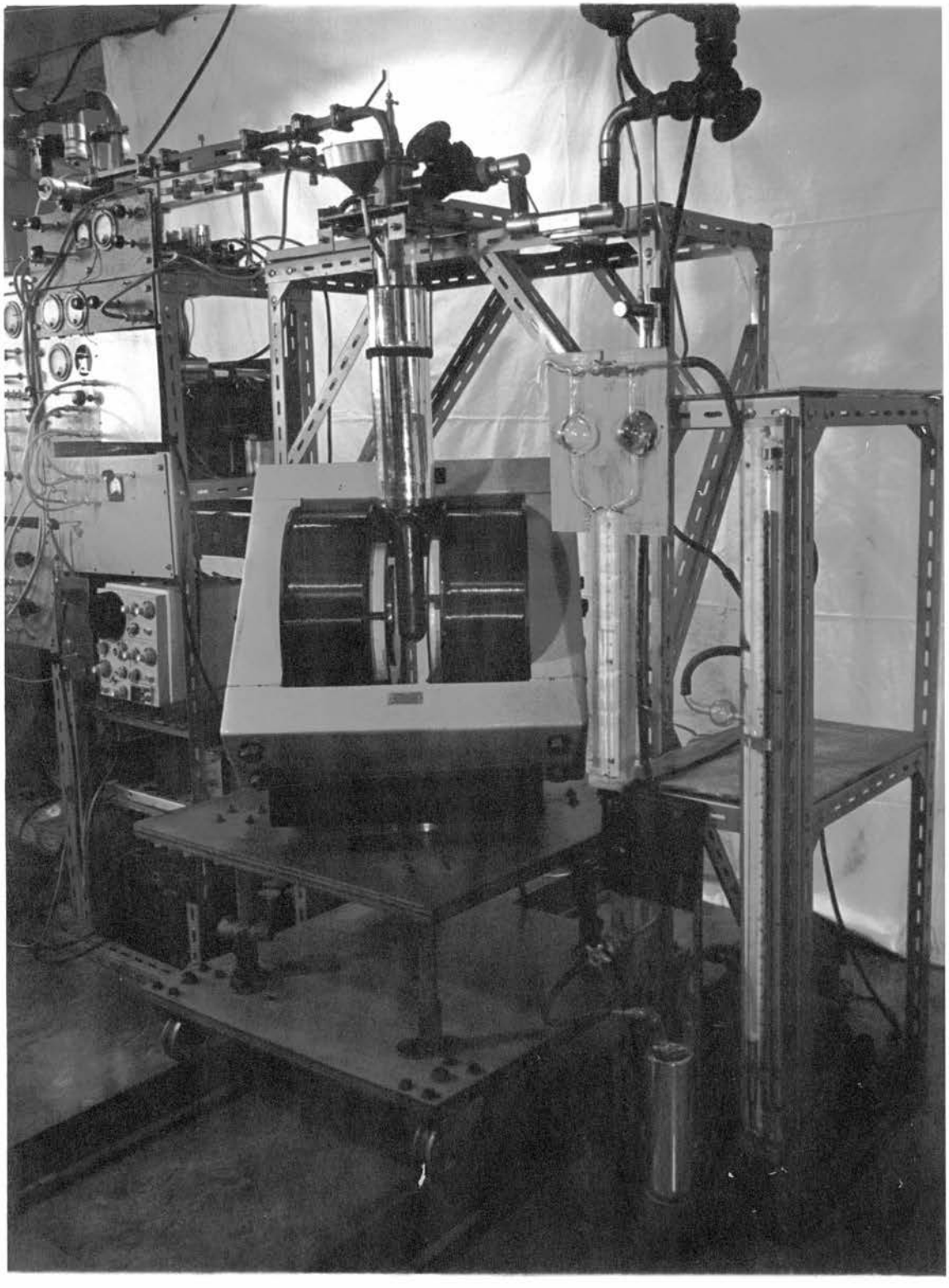

Fig. 6. Magnet and Cryostat.

The reflectionless loads were first adjusted for minimum V.S.W.R. and the position of the wooden fish-tail pegs set with wax. Each crystal mount was then tuned by means of the capacitive screws and the variable shorting plunger for the same condition. Any change in the operating frequency of the spectrometer or in the characteristics of the crystals could easily be accommodated by a small variation in the position of the plunger.

When the magic tees were tuned the actual conditions of use in the spectrometer were applied, i.e. either a matched load or a crystal mount was connected to arms 1 and 2 as required. The tuning screws on the E- and H-arm were then adjusted for a minimum standing wave ratio. By using another crystal mount the isolation property of the E- and H-arms of the tee could be measured.

For each of the reflectionless loads a V.S.W.R. of less than 1.035 was achieved, and for the crystal mounts, the V.S.W.R. is less than 1.05. With the magic tees the H-arm could be tuned to better than 1.03 but with the E-arms could only be tuned to a V.S.W.R. of about 1.2.

3.4. The Cryostat.

As the actual transfer of liquid helium into the cryostat takes place at the liquifier the whole cryostat has to be easily detachable from the rest of the apparatus. The cryostat is shown in Figure 6 and a schematic diagram, Figure 7, is also included. A detailed description now follows.

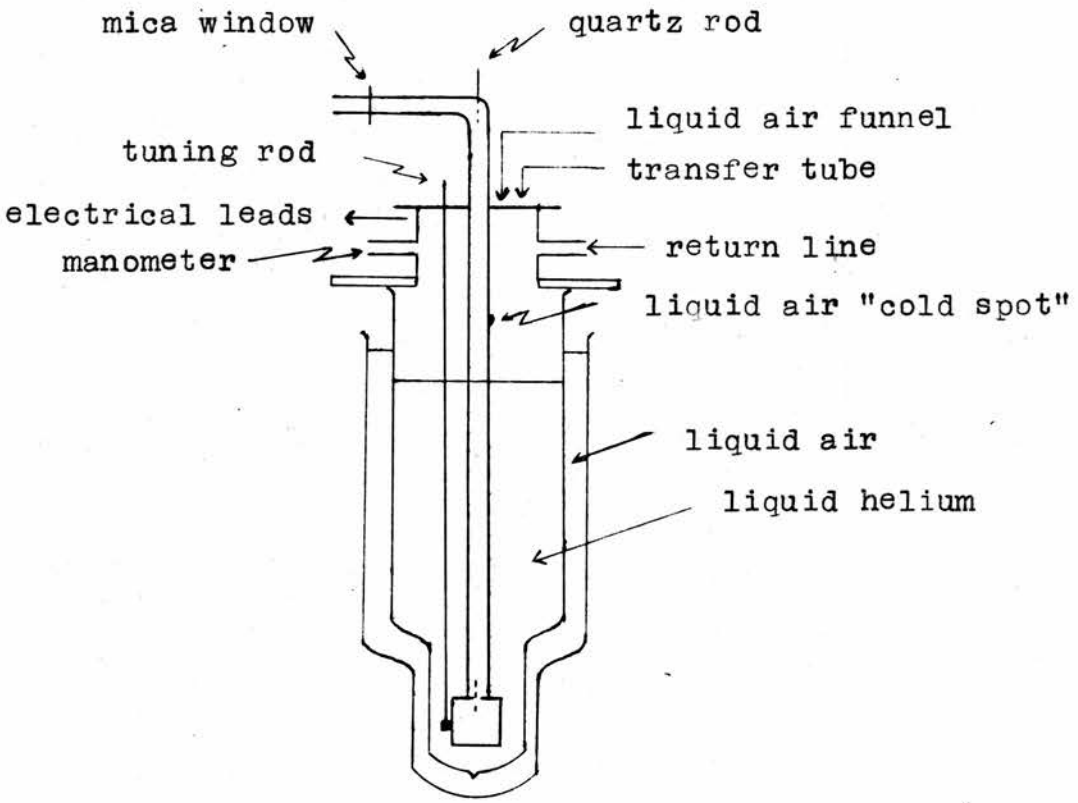

Fig. 7. Cryostat (schematic).

3.4.a) Glass Dewars.

A double-dewar system is used, and this presents a problem as the maximum air gap in the magnet was 2 $\frac{5}{16}$ in. (58.74 mm.). Into this space four thicknesses of glass with interspaces between each has to be fitted, and the diameter of the inner surface of the helium dewar has to be greater than 31 mm. if the cavity and tuning mechanism are to be accommodated. Thus the accuracy of construction of the lower section of the dewars is very critical. The upper dewar sections are not restricted in thickness or diameter, however, as will be seen in the schematic drawing. Monax glass is used throughout.

The liquid helium dewar.		Dimensions.
Tail -	Wall thickness	0.5 mm.
	Inner Wall	34.5 mm. O.D.
	Outer Wall	37.5 mm. O.D.
	Length	20 cm.
Main Body -	Wall thickness	1 - 2 mm.
	Inner Wall	55.5 mm. O.D.
	Outer Wall	69.0 mm. O.D.
Overall length		70.5 cm.
Capacity		1 litre.

The upper 12.5 cm. of this dewar is single walled with a rim (0.5 cm.) at the top. A brass collar with a Gaco ring cushion is slipped over the dewar and clamped to the top plate by three OBA screws, the upper surface of the rim butting onto another Gaco ring. The double walled section of the dewar is

silvered except for two diametrically opposite vertical strips (½ in. wide) for observation purposes. This dewar is left slightly soft (5 mm. air pressure) to facilitate pre-cooling. When filled with liquid helium this air in the interspace solidifies and thus there is no loss in efficiency as heat insulation is maintained. As Monax glass is slightly permeable to helium it is necessary to repump this dewar after ten or twelve runs.

Liquid Air Dewar.		Dimensions.
Tail -	Wall thickness	0.5 mm.
	Inner Wall	40.5 mm. O.D.
	Outer Wall	44.5 mm. O.D.
	Length	21.5 cm.
Main Body -	Wall thickness	1 - 2 mm.
	Inner Wall	89.5 mm. O.D.
	Outer Wall	101.5 mm. O.D.
Overall length		61.3 cm.

This dewar is supported by a wire cage which fits round a raised section of the dewar about 10 cm. from the top. The upper ends of the cage pass through three holes in the top plate and are held by knurled nuts. Thus a fine adjustment of the clearance between the two dewars can readily be achieved. The interspace is silvered and pumped hard.

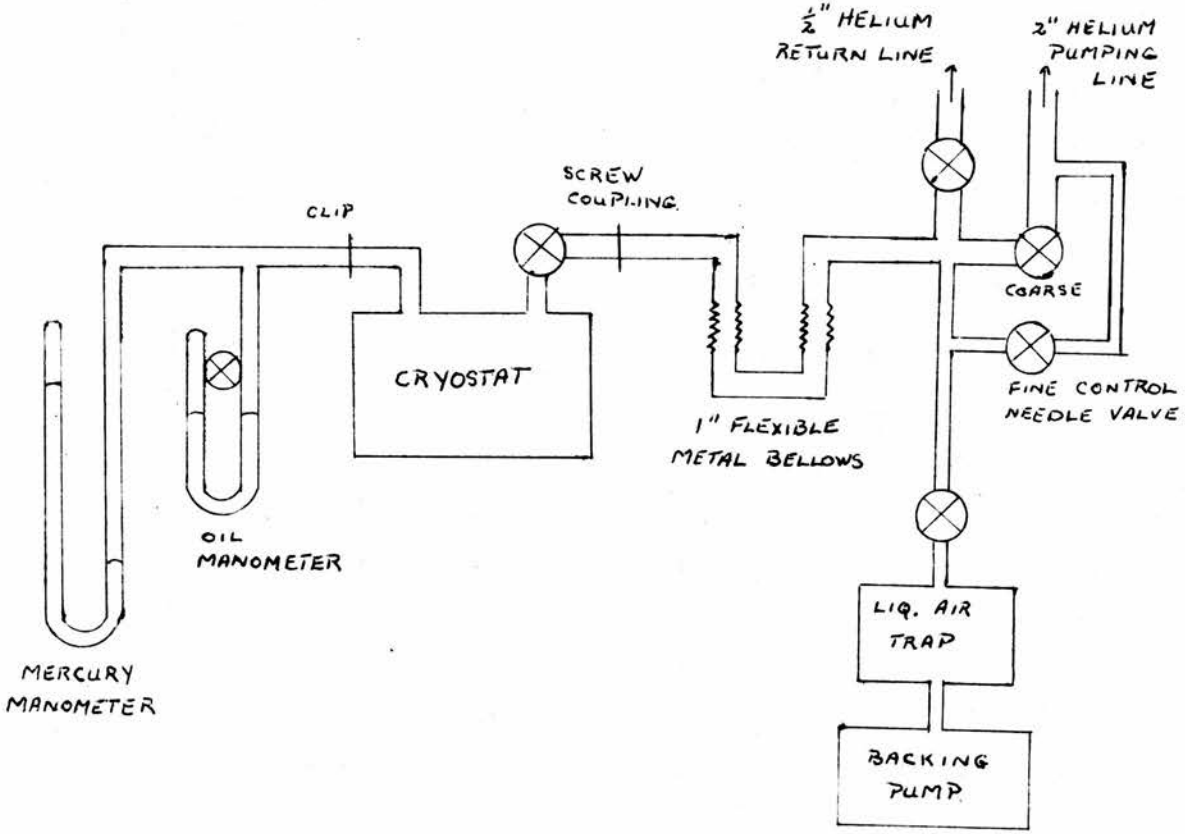

Fig. 8. Vacuum System (schematic).

3.4.b) Construction of the Cryostat Head.

The top plate of the cryostat is a brass plate 8 in. x 6 in. x ¼ in. which is clamped by four OBA winged nuts to a "Handy Angle" frame which spans the rails for the magnet trolley. The two supporting members of this frame protrude 6 in in front of the main frame, and are fixed at a height of about 5 feet from the floor. Thus, the dewars can be fitted in situ and the whole cryostat assembly can be lowered directly into position over the four OBA screws. These also act as levelling screws. A section of brass tube 2⅜ in. I.D. x ⅛ in. thick is fitted into the top plate with its vertical axis through the centre of the plate and protruding ½ in. down from the lower side of the plate. This part under the plate acts as a guide when fitting the inner dewar. A brass ring, 3½ in. O.D., is soldered to the top of the brass tube and a brass plate (the top-cap), of the same diameter and stepped for a Gaco ring is clamped to this ring by six 2BA screws. This gives a vacuum tight seal and the top-cap acts as a support for the waveguide assembly and other fittings.

Because of the necessity to recover all the helium gas, the helium circuit must be a closed one. The whole circuit (and pumping system) is shown in Figure 8. A 1 in. copper tube inserted into the side of the section of 2⅜ in. I.D. x ⅛ in. brass tube serves both as a direct helium gas return line to the storage balloon, and as a pumping line should an operating temperature below the boiling point be required. Included in

this line from the cryostat are a 1 in. Saunder's valve used to seal off the cryostat when it is carried to and from the liquifier, and a screw coupling where the cryostat can be disconnected from the line. On the fixed side of this coupling there is a double bellows system, the bellows being in the vertical arms of a U-shaped section to avoid any lateral pull on the cryostat as they contract on reducing the pressure in the system. They also prevent any vibrations from the pump side of the line being transmitted to the cryostat. The bellows section leads into a T-junction between the ½ in. helium gas return line to the storage balloon and the main 2 in. pumping line, each line being fitted with a Saunder's valve. To give a fine control of the pumping speed a needle valve is included, by-passing the large 2 in. valve through a length of 6 mm. Cu-Ni tubing. Into this tubing is set a T-section giving entry to the line for a rotary vacuum pump used in the evacuation of the system prior to a helium run. This pumping line includes a valve and a liquid air trap.

A second entry into the side of the main brass tube in the cryostat head leads to a mercury manometer. This measures the vapour pressure of the helium gas above the helium liquid level and is used to determine the operating temperature, the relationship between pressure and temperature being given in a table from Physica[49]. Small changes in pressure are read on a differential butyl phthalate manometer connected in parallel with the mercury manometer. As this entry to the Cryostat also

serves as a return line for the helium gas boiled off during a liquid helium transfer, it is made of double walled Cu-Ni tubing.

A heater of insulated Eureka, 32 SWG wire is wound on the bottom of the waveguide section in the dewar, this being used to speed up the boiling off of any liquid helium left at the end of a run. The leads from this pass up the outside of the waveguide and are brought out through a third tube in the side of the brass tube in the cryostat head. Kovar seals are used to give a vacuum tight connection.

There are several entries to the cryostat through the top-cap besides the waveguide entry through its centre which is described in Section 3.4.c).

During the transfer of liquid helium the transfer tube passes through a $\frac{1}{2}$ in. threaded Cu-Ni entry. This transfer tube must pass well down into the dewar, and as a guide for it a length of Cu-Ni tubing was soldered to the side of the waveguide. Normally this entry is sealed off by a rubber stopper and, should any over-pressure build up inside the dewar, this will blow off and act as a safety valve.

The second opening in the top-cap is used as an exit tube for 10 cc. liquid air reservoir of Cu-Ni tubing. The bottom of this reservoir is 'tied' to the entrant waveguide at a point 16 cm. below the top-cap, thereby fixing the temperature at that point. This means that the thermal gradient along the section of waveguide above the liquid helium level is decreased

and liquid helium is conserved. This device will be most effective when the liquid helium level is low, but in practice it did not appreciably increase the running time. The design was based on data given in reference (50).

The third opening is for the $\frac{1}{16}$ in. stainless steel tuning rod of the cavity tuning mechanism. This rod passes through a Gaco disc held down by a screw cap. A knurled knob is clamped to the rod to facilitate tuning.

As stated the whole cryostat head has to be disconnected and carried to the helium liquifier for filling. The actual transfer is very economical, approximately 230 litres of helium gas at N.T.P. being expended to cool the cryostat system from liquid air temperature and the transfer tube from room temperature, and a further 470 litres being expended in the actual transfer. Running time is adequate, being upward of twelve hours depending on operating temperature and changes in operating temperature.

3.4.c) Waveguide Assembly and Thin-walled Waveguide.

The E-plane waveguide bend leading from the microwave bridge enters cryostat through a bush consisting of a 1 in. length of standard British waveguide set in the centre of the top-cap. The internal dimensions of this are the same as the external dimensions of the waveguide leading into the cryostat.

To reduce the heat leak in the cryostat it is necessary to use waveguide other than the normal brass type for the length inside the dewar. A length of waveguide of 0.012 in. wall

thickness, drawn from Cu-Ni tubing, is used by fitting this with a brass collar at the top to bring its outside dimensions up to the normal waveguide size. Then this section and the length of the E-plane bend protruding into the cryostat are butted together under another collar of British waveguide. The whole assembly is soft soldered. Thus only the top 2 in. of waveguide inside the cryostat was of the normal brass type, the rest of the length to the cavity being of thin-walled Cu-Ni waveguide. This reduces the possible heat leak by a factor of about 20, but some sacrifice is made for this in that the Cu-Ni waveguide does not have so accurately rectangular dimensions as the normal brass tube. The cavity is soldered directly on to the bottom of the thin-walled waveguide.

Since liquid helium is allowed to enter the cavity and the thin-walled waveguide, a vacuum seal must be included somewhere outside the cryostat head. Another requirement is that the waveguide must be readily detachable when the cryostat is removed to be filled. These requirements were met by the insertion of a thin mica window clamped between the Gaco rings in two plane-faced waveguide couplers close to the bend in the waveguide at the top-cap, and the inclusion of a length of Sander's flexible waveguide coupled to the cryostat assembly by means of a quick-release spring clamp. This also serves to prevent any vibrations and microphonics from being transmitted to the microwave bridge.

A fine tuning mechanism is also included in the cryostat assembly, requiring another vacuum seal. This is a $\frac{1}{8}$ in. diameter quartz rod passing through a hole in the broad face of waveguide bend into the top-cap, right down the inside of the waveguide and into the cavity through the coupling hole. At the top of the waveguide bend a brass block is soldered in position, this block being threaded and a seat cut in it for a Gaco hat-gland. The quartz rod passes through this hat-gland and the screw which clamps the hat-gland in position, the rod being cemented to another screw to enable it to be raised or lowered as required. The whole assembly constitutes a good vacuum seal.

3.5. The Resonant Cavity.

A prime consideration in the design of the cavity is the space available inside the tail of the helium dewar, the inner surface diameter being about 33 mm. The inclusion of a tuning mechanism cuts this down still further and some clearance has to be left to allow liquid helium to pass into the small reservoir under the cavity. With all these considerations in mind the cavity resonator was designed using the data given in references (51) and (52).

3.5.a) Design.

It was felt a cylindrical cavity would be easier to fabricate, and with the diameter, D, being fixed to less than 30 mm. and the length of the resonator, L, equal to one guide

wavelength the choice of operating point on the Mode Chart[51][52] was limited. It was obvious that a cylindrical cavity with a TE 011 normal mode would be too large, this being the cavity which requires minimum volume for a given Q-value and resonant wavelength. Thus the cavity chosen must have a limited Q-value. The TE 111 mode was chosen as the one satisfying the special requirements and the one least likely to give trouble from degenerate modes.

The fundamental equation from which the mode chart is derived is

$$(fD)^2 = A + Bn^2\left(\frac{D}{L}\right)^2$$

where

f = frequency in Mc/s.
D = diameter of cavity in inches.
L = length of cavity in inches.
n = number of half wavelengths along the cylinder axis.
A = a constant depending on the mode, involving the corresponding root of a Bessel function.
B = a constant depending on the velocity of e.m. waves in the dielectric.

As the cavity was to be tunable about a centre frequency of 9375 Mc/s., the ratio $(\frac{D}{L})$ was chosen to satisfy special conditions so that no unwanted mode of oscillation would be included in the tuning range. Such a value for $(\frac{D}{L})^2$ was 0.4 giving a diameter of 0.830 in. and a length of 1.315 in. for a working frequency of 9375 Mc/s. As this cavity has only one closed loop of r.f. magnetic field, the regions of maximum

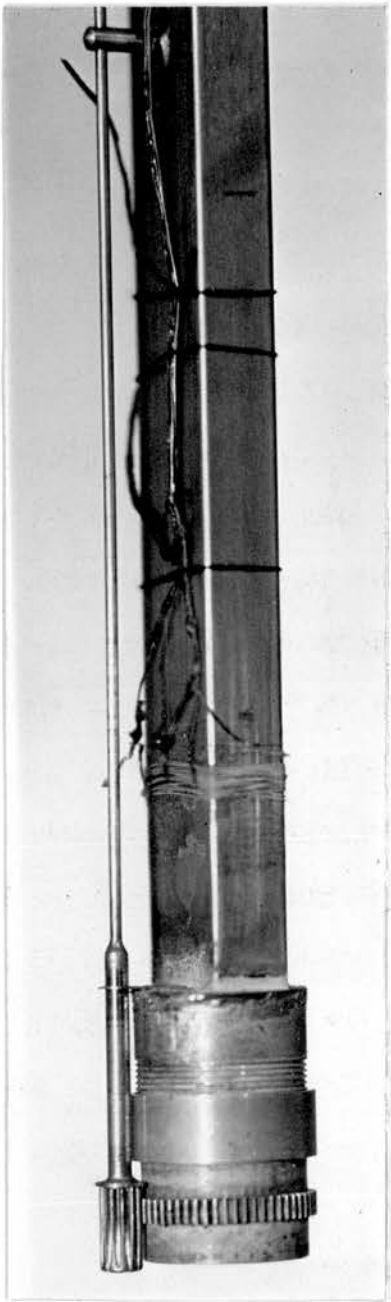

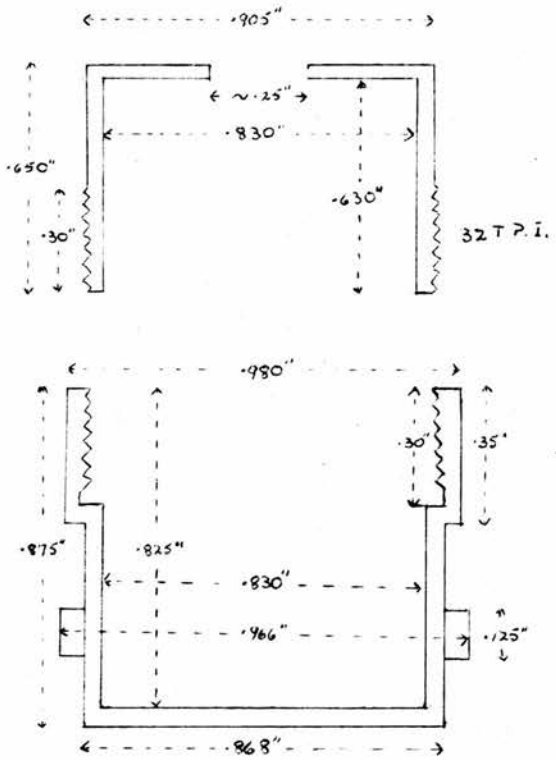

Fig. 9. Cavity (photograph and schematic).

magnetic field occur in the centre of the top and bottom faces. Thus the sample need only be placed on the bottom of cavity to be in a centre of maximum r.f. magnetic field, it being fixed in position with nail varnish. The normal-mode field equations are given in reference (52).

3.5.b) Construction.

The values worked out above for the diameter and length of the cavity were for a cavity in air, and allowance had to be made for the dielectric medium being liquid helium (dielectric constant = 1.048 at the boiling point) and for any contraction in the dimensions due to a reduction in the temperature. Such changes of resonant frequency were within the tuning range.

The construction of the cavity is in the form of two cylindrical cups turned out to close tolerance from 1 in. brass stock and screw cut to form a right cylinder of variable length. (Figure 9). This method of joining the two sections of the cavity does not greatly increase the losses in the walls. The inner surfaces are silvered and polished to reduce the skin depth which is included in the mode-shape factor $Q\frac{\delta}{\lambda}$. Great care was taken in the manufacture to avoid any work stresses being set up in the walls.

The final dimensions chosen are:-

Internal diameter	= 0.830 in.
Maximum length	= 1.45 in.
Minimum length	= 1.15 in.
Average wall thickness	= 40/1000 in.
Coupling thread	= 32 T.P.I.
Tuning range	= 9.1 kMc/s. - 9.6 kMc/s. for helium at 4°K.
Medium	= silver-plated brass.

Tuning by changing the length of the resonator is arranged by a geared drive from the stainless steel rod, extending from the cryostat top-cap through four small bearings soldered to the entrant waveguide. On this is mounted a small gear wheel which drives a larger wheel slipped over the lower half of the cavity giving a reduction drive of 1 to 5. Stops are supplied at both ends of the driving wheel. The tuning range achieved by this is 500 Mc/s. about a centre frequency of 9350 Mc/s. For a reduction in temperature from room temperature to 4°K., and for a change in dielectric medium from air to liquid helium, the change in resonant frequency is about 160 Mc/s which is well within the tuning range. Because of the length of the driving rod, the torque which can be applied to the cavity is limited. Thus the screw thread on the cavity has to be reasonably loose. However it should not be too free, since the pressure from the tuning mechanism may tilt the bottom half of the cavity, giving a change in matching conditions of the cavity arm. This can lead to a spurious resonance.

For fine tuning an $\frac{1}{8}$ in. quartz rod is fitted through the E-plane bend at the top of the cryostat and passing through the cavity coupling hole to penetrate into the cavity to a maximum depth of 0.6 in., as described in Section 3.4.c). The sensitivity of this tuning is 4 Mc/s per turn of quartz rod giving an overall range of 60 Mc/s which is slightly greater than the electronic tuning range of the klystron used. The coupling hole is cut to accommodate this rod and prevent any excessive lateral movement of the section inside the cavity.

3.5.c) Coupling and Q-Value.

The whole cavity assembly is soldered on to the end of the thin-walled waveguide section, with a 0.01 in. plate in between the two parts. The coupling hole was cut in this plate. The cavity mode is excited from the end of the waveguide via an iris, a type of coupling which is largely magnetic, the electric vectors in the waveguide and in the cavity being polarised in the same direction. Because of a slight asymmetry which occurred somewhere in the cavity construction trouble was experienced from a doubly-degenerate mode. To split these modes completely and remove the unwanted mode away from the operating region, the coupling hole in the thin plate was cut as a narrow slot about $\frac{5}{16}$ in. long and mounted in direction parallel to the H-plane of the entrant waveguide. The size of the slot was the final variable in the choice of the optimium coupling value. The size of hole was gradually increased and, by displaying the

cavity response on the oscilloscope, the cavity dip was observed to increase as the hole was enlarged (undercoupled state) until it reached a maximum at critical coupling, and then diminish again (overcoupled state). Because the cavity becomes more strongly overcoupled as the temperature is reduced, due to a decrease in the losses and a corresponding increase in the Q-value, the selection of the coupling at room temperature was no criterion. Trial showed that satisfactory results were obtained with a slightly undercoupled cavity at room temperature. The sliding stub tuner is the only available external control of the coupling. Unwanted effects could also arise if the top plate of the cavity was too thick. To avoid this the top surface was turned down to about 0.02 in. giving a total thickness at the coupling hole of about 0.03 in. The actual coupling factor and Q-value of the cavity can be measured by inserting a Standing Wave Indicator in the cavity arm of the microwave bridge. A full treatment of such measurements is given in references (53) and (54).

From the dimensions of the cavity, the skin depth of the plating medium, and the resonant frequency, the expected Q-value was worked out from equations given in reference (51). This was found to be of the order of 100,000 but such a value cannot be achieved in practice.

By measurement it was found that:-

At Room Temperature -

Loaded Q = 3,500
Unloaded Q = 5,700
V.S.W.R. = β = 0.625 = $\frac{1}{r}$ - undercoupled state.

At Helium Temperatures -

Loaded Q = 6,500
Unloaded Q = 10,000
V.S.W.R. = β = 0.54 = r - overcoupled state.

3.6. The Magnet.

With a spectrometer designed to operate in the X-band at a frequency in the region of 9375 Mc/s. a d.c. magnetic field of approximately 3,500 gauss is required for the Zeeman splitting of the energy levels. Such a magnet was designed in this laboratory in collaboration with Newport Instruments Limited (Figure 6). This has since been developed as their standard H-type 7 in. magnet.

Dimensions:-

Outside length of Yoke	= 23 in. x 23 in.
Cross-section of Yoke	= 7 in. x 3½ in.
Diameter of Pole Pieces	= 7 in.
Gap width	= 2 $\frac{5}{16}$ in.
Weight of magnet and mount	≈ 11 cwts.
Cross-section of rectangular wire	= 0.05 in. x 0.015 in.
No. of turns per coil	= 1850
Resistance of coil in series	≈ 12 ohms
Power dissipation in coils	≈ 300 watts
Field range	= up to 6,000 gauss (intermittent operation)

3.6.a) Assembly.

The magnet is mounted on a trolley which was made in the laboratory, as was the rest of the mount, and runs on a set of 4 in. angle iron rails, as the one magnet has to serve three experimental stations. The yoke is supported on a cradle at an angle of 45° to the vertical, the whole assembly rotating on a ball-race about a vertical axis through the centre of the magnet gap. The outer rim to the ball-race is graduated in degrees so that any angle of the magnet relative to the forward position can easily be set.

3.6.b) Alignment.

The magnet was assembled in the laboratory according to the manufacturers instructions. The mechanical alignment was checked by testing the pole faces for parallelism, and by adjustment and measurement with a clock gauge, they were finally adjusted to parallelism within an accuracy of 0.0004 in.

3.6.c) Sweep Coils.

Two pairs of sweep coils have been used. These are mounted on the pole caps and screwed to the outside faces of the main coil bobbins. The original pair were wound in the laboratory on brass bobbins using 2,900 turns of 26SWG insulated copper wire, and an insulating layer of paper on each bobbin. These proved to be too noisy acoustically and were a source of microphonics.

The Newport Company made new coils with 3,500 turns on each on bakelite formers. A current of 0.2 amps through these coils connected in parallel gives a modulation field of 50 gauss at 50 c/s.

3.6.d) Power Supply.

Originally the magnet current was drawn from a bank of twelve 12v. lead-acid accumulators. These cells could be used as two banks of 75v. each, or as one of 150v., the current being controlled by a series of rheostats in series with the magnet coils. The batteries were charged by a built in rectifier at currents up to 6 amps., and could be trickle-charged while in use. This system suffered from the disadvantage that the magnet current was never steady due to the fall off in battery voltage, unless operating under a trickle-charge condition. Even this was unsatisfactory due to the large heat capacity of the coils, the field drift being estimated as 0.5 gauss/min.

These batteries were replaced a few months ago by two stabilised supply units, Newport Instruments Limited, Type B. The current stability claimed for these is 1 part in 10^4, or a field ripple of 0.5 gauss peak-to-peak, and they give continuous variation with both a course and a fine control over the full range of current from 0 to 12 amps. As these have a stabilised output the magnet current is independent of the change in the resistance of the coils when warming up.

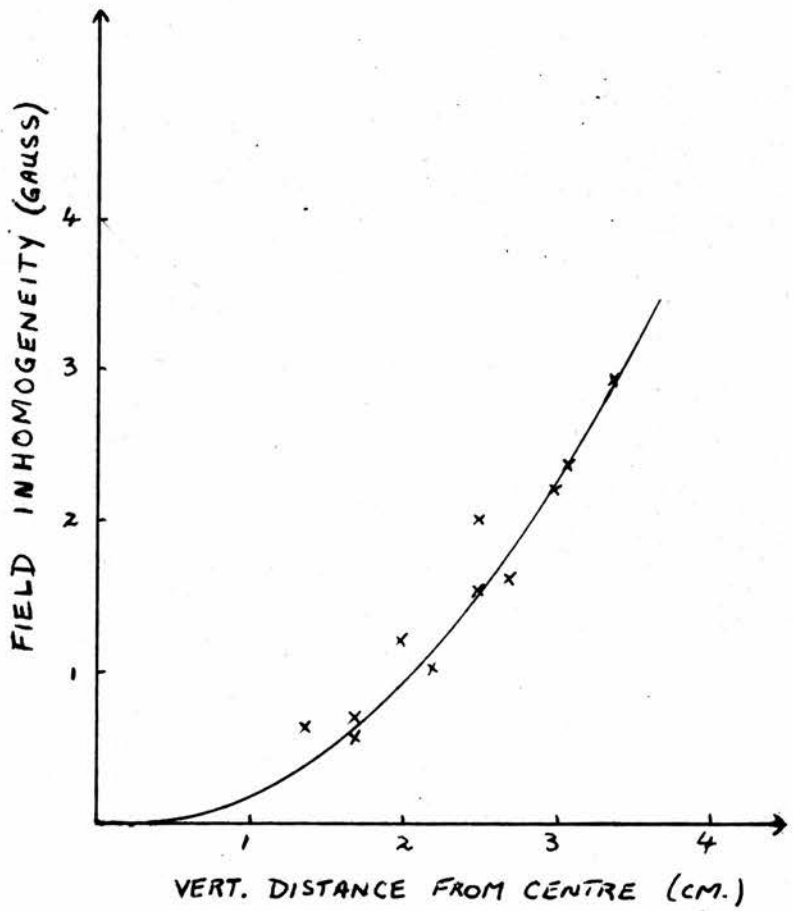

Fig. 10. Magnetic Field Homogeneity Graph.

3.6.e) Homogeneity.

The magnetic field homogeneity was checked using a nuclear magnetic resonance method by Lowe[55], the unit being built in the laboratory by Mr I.M. Firth. The moveable probe consists of a small coil immersed in glycerol fed from a variable oscillator, and the frequency of the oscillator is adjusted until the nuclear magnetic resonance line appears on the oscilloscope. By examining the frequency variation for movements of the probe vertically and horizontally along the magnetic axis, and across the magnet gap, the magnetic homogeneity can be plotted. Figure 10 shows the homogeneity plot for points vertically below the centre of the magnet gap in a plane parallel to the pole faces and equidistant from each. Field differences of 0.25 gauss could be detected by this unit, but these results were taken with the battery power supply. Assuming better stability with the stabilised power supply, the field drift across the gap along the centre axis of the pole pieces will be better than 2 gauss, i.e. better than 0.35 gauss over the sample, and the homogeneity at the centre of the gap within a sphere of radium 2 cm. will not be worse than 0.5 gauss.

3.7. Mounting of Microwave and Electronic Equipment.

Initially thought was given to the mounting of both waveguide components and electronic units, taking into account the space available and the ease of access required for each component. As it was felt easy servicing of electronic units without removing them from the apparatus would be required, all circuits are built on plates of tinned-iron or aluminium and mounted vertically on a rack constructed of "Handy Angle". If necessary, each unit can readily be removed for any major rebuilding. This rack also serves as a base for the mounting of the microwave bridge, this being held by brass clamps screwed to a wooden top deck. Small adjustments of height can be accommodated by flexibility in these clamps.

The actual layout of electronic units on the rack was considered, and all power supplies are mounted on the rear as they require no attention in the normal course of events. The other units are mounted with all controls and components to the front and valves to the back of the plates. Screening, where necessary, could easily be effected by fixing boxes or plates to each unit to cover all components and wiring. Other items, such as H.T. batteries and Ni-Fe heater batteries are laid out on horizontal shelves within the frame.

3.8. The Electronics.

3.8.a) Power Supplies.

Each supply has been built for different operating voltages and currents depending on the requirements of their corresponding loads, but the same basic design is used in each. This includes a mains transformer, a valve rectifier and a condenser-choke input filter followed by a negative feed-back d.c. regulator. The current handling requirements determine the number of series valves used, though latterly one 12E1 valve has been preferred to a stack of EL84 valves. The actual current control in the supply is determined by the grid voltage of these valves. The d.c. amplifier consists of a balanced-input difference amplifier cascaded by another difference amplifier with its grid fixed at some reference voltage. The output voltage can be no more stable than the stability of the reference voltage, but a gas-discharge tube is adequate. The supply end of the anode resistor of the last stage of the d.c. amplifier is connected to the unstabilised side of the current control valve, thereby ensuring a reasonable gain for this stage when the grid voltage is close to the cathode voltage. In each power supply a variable resistance is included in the potential divider for fine tuning of the output voltage about the optimum design voltage. The noise voltage on the output supply when operating under normal loading conditions is less than 2mv. r.m.s. in all cases.

The power packs included in the apparatus are:-

(1) 0 to - 500v.; anode-cathode voltage for the Varian X-13 signal klystron (Figure 4). This was the most troublesome to develop due to the high voltage ratings demanded of the components.

(2) 0 to - 350v.; anode-cathode voltage for the local oscillator klystron (Figure 5).

(3) 0 to + 250v.; H.T. voltage for the I.F. Amplifier and the modified strip used as a pre-amplifier for the A.F.C. circuit.

(4) 0 to - 600v.; H.T. voltage for the single valve d.c. amplifier in the A.F.C. circuit. This has a further tapping for a 0 to - 300v. output.

3.8.b) I.F. Amplifier.

The choice of intermediate frequency was determined mainly by the availability of a modified "Pye" television amplifier with a 10% bandwidth centred on 45 Mc/s. The circuit consists of a low impedance input and five stages of stagger-tuned amplification[56] using EF50 pentodes, followed by a diode detector (EA50) and a low impedance cathode follower

output (EF50). Current jacks were added so that the detecting crystal current from the microwave bridge, and the second detector current from the I.F. amplifier can be monitored by means of two milliammeters. The overall gain is controlled by the addition of both a course and a fine control of the grid potential of the first four amplifying stages, using a 9v. grid-bias battery, and a screen grid potential control on the last three stages of amplification, the latter being necessary due to the relatively sharp cut-off in the valve characteristics. The gain of the amplifier is estimated as greater than 30db. at the saturation point.

A large 50c/s ripple occurred on the output of the I.F. amplifier when the heater current was drawn from a 6.3v. transformer. This was replaced initially by a bank of Ni-Fe cells and finally by an Advance Components 6.3v. d.c. supply. The H.T. is supplied by a + 250v. power unit, the current drain being approximately 100mA. Under proper operating conditions the amplifier output contains less than 5mv. peak-to-peak 50c/s ripple, and the high frequency noise is cut down by connecting an R.F. filter on the output.

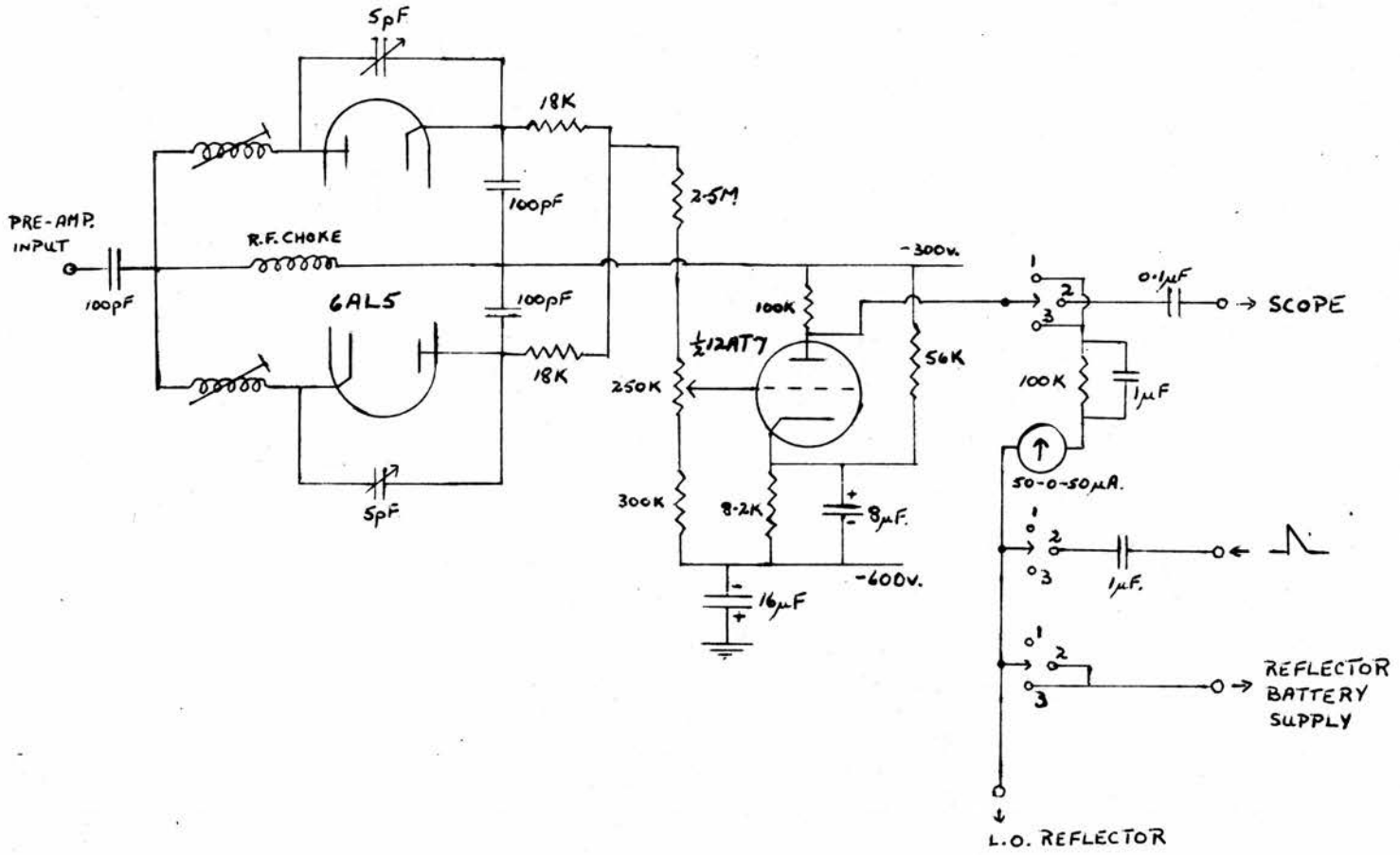

Fig. 11. Discriminator and A.F.C. Circuit.

3.8.c) Automatic Frequency Control.

The essence of superheterodyne detection is that the local oscillator output must be 45 Mc/s less, or greater than that of the signal klystron output, otherwise the I.F. output level varies. The signal klystron is tuned to the resonant frequency of the cavity and is relatively stable. Thus any drift in the I.F. is due to a change in output frequency of the local oscillator. Control of this is by applying a correction voltage to the reflector of this klystron.

At the input to the I.F. amplifier, part of the signal is taken out and fed into another modified "Pye" strip with the same centre frequency as the signal amplifier. Only the first five stages of stagger-tuned amplification are used, with gain controls similar to those on the I.F. strip. The output is taken from the tuned load on the final stage and fed into the discriminstor shown in Figure 11. The two resonant circuits in the discriminator are tuned to resonate at frequencies one above and one below the correct intermediate frequency, and the d.c. potentials developed across the diode output condensers have magnitude and sign depending on the difference between the input frequency and the correct intermediate frequency (57)(58). These voltages are fed into the grid of a d.c. triode amplifier (59) whose anode potential is variable about the reflector potential. The output from this amplifier is then fed to the reflector by means of a multi-pole ganged switch.

Position 1 is used to adjust the reflector and control output voltages to the same value with no signal being fed into the discriminator. In position 2 the control loop is broken, and a low frequency saw-tooth sweep is applied to either the signal or oscillator klystron reflectors. This is giving a frequency sweep of the output of the microwave bridge and shows on the oscilloscope the S-shaped correction curve at the discriminator output (Figure 12c). The frequency separation of the peaks of this curve is about 3 Mc/s, and the peak-to-peak voltage can be controlled by the gain of the pre-amplifier. At position 3 the control circuit is complete, and if the potentials have been set up correctly, the operating frequency will be the centre frequency of the I.F. amplifier.

3.9. Scope Display and Valve Voltmeter.

Frequency modulation of the output of either klystron is achieved by the application through an R-C circuit of a low frequency saw-tooth sweep voltage to the klystron reflector. This sweep is not large enough to present the whole mode of the signal klystron on the oscilloscope, but the display of the centre of the mode is sufficient for lining up the klystron frequency to the resonant frequency of the cavity. Visual presentation of the whole mode for the thesis (Figure 12a) was by a larger peak-to-peak 50c/s sinusoidal voltage which swept through the full mode twice in every cycle. The saw-tooth sweep was large enough to display the whole local oscillator mode.

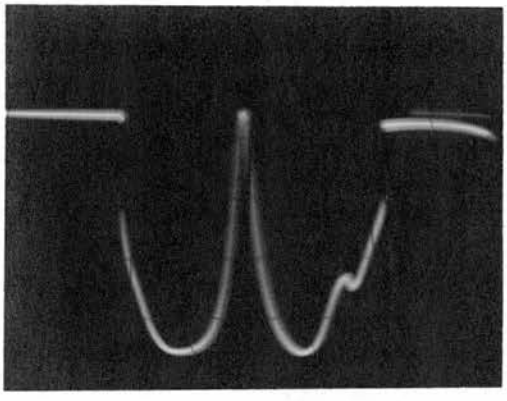

a) X-13 klystron mode display showing matched cavity dip and smaller wavemeter dip.

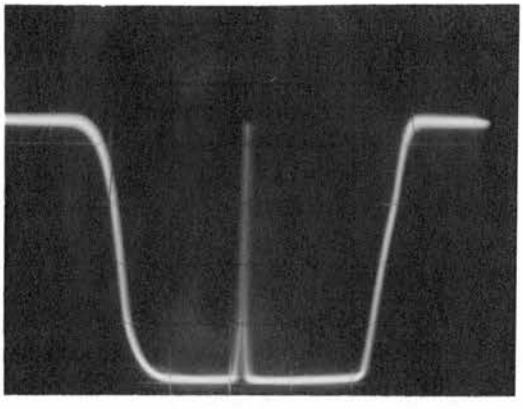

b) I.F. Amplifier Response Curve showing cavity dip.

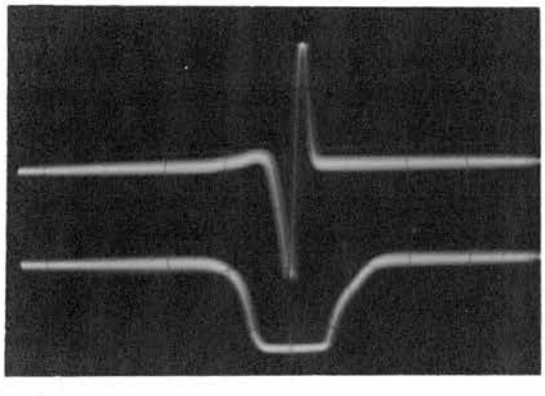

c) I.F. Amplifier Response Curve and A.F.C. Correction Curve.

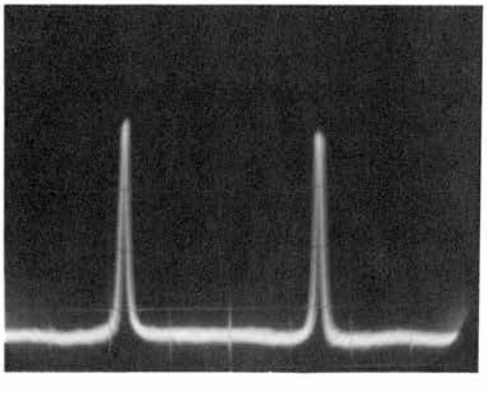

d) D.P.P.H. Resonance at room temperature.

Figure 12.

When the klystrons are operating at constant reflector voltage the coupling condensor is connected to earth to provide R-C integration at the reflector. This prevents any unwanted voltage instability affecting the output frequency.

All observations are made at the detecting output crystal and typical examples are shown in Figure 12.

(a) The reflected pattern from the cavity arm is displayed for the whole klystron mode using a 50c/s sinusoidal sweep on the reflector of the signal klystron. This shows a dip for the matched cavity and a smaller dip due to the wavemeter cavity resonance. The sharpness of the main dip is an indication of the Q-value of the cavity.

(b) The I.F. amplifier response curve with the cavity dip in the centre is shown here, the synchronised sweep being applied to the signal klystron. Thus the second detector current will be a minimum when the cavity dip is in the centre of the response curve.

(c) This is the display of the I.F. amplifier response curve and the A.F.C. output on a double-beam oscilloscope with the synchronised saw-tooth sweep applied to the local oscillator reflector. The peak-to-peak value of the A.F.C. curve is 40v.

(d) The video display of a large D.P.P.H. sample (10^{18} spins) is achieved by applying a large amplitude 50c/s magnetic modulation on the sweep coils of the magnet. A phase shifter and Z-modulation of the oscilloscope trace is used in this display.

A valve voltmeter is used as the monitor of the intensity of the absorption signal during the actual sequence of runs. It is essential that the power level be the same in each run, under the same conditions of input power and attenuation in the detecting arm and local oscillator power, if the results are to be co-related. The actual adjustments of the two calibrated attenuators are such that the same reading on the valve voltmeter is achieved at all settings, i.e. any increase in the incident power is compensated for by an increase in the attenuation in the detecting arm.

CHAPTER IV.

Operation and Results.

Introduction.

The main work for this thesis has been the study of the temperature dependence of the spin-lattice relaxation time of sample D29 as described in Section 2.8. The temperature range covered has been from 4.2°K. down to our lowest attainable temperature of 1.17°K.

This Chapter is a report on the performance and sensitivity of the apparatus, the details of the setting-up procedure and the results obtained. The concluding Section outlines future studies and developments possible with this apparatus.

4.1. Spectrometer Sensitivity.

To determine the sensitivity of the spectrometer resonance experiments were carried out with a crystalline sample of the standard free radical marker D.P.P.H. (diphenylpicrylhydrazil) which has a g-value of 2.0036 and a line width of 2.7 gauss. A series of samples were made up in the laboratory with free spin concentrations from 10^{18} down to 2×10^{14} spins, all in the form of closed perspex pill-boxes with central holes of diameter 1mm. or 2mm. The sample used to calibrate the apparatus at room temperature contained about 2×10^{18} spins.

The main factor limiting the sensitivity is the inherent noise in the I.F. amplifier. Most of the 50c/s noise was removed by running the valve heater from a 6.3v. d.c. supply, but not all the r.f. noise components could be removed by connecting a low-pass R.C. filter across the amplifier output. Other considerations in calculating the sensitivity are the Q-value of the cavity, saturation effects, crystal noise and microphonics. With experience in setting up and operating the apparatus, many of these effects can be minimised.

In the experimental estimation of the sensitivity the D.P.P.H. sample containing 10^{18} spins is placed in the region of maximum r.f. magnetic field in the cavity, and the resonance is displayed on the oscilloscope by means of a 50c/s magnetic field modulation (Figure 12d). The signal to noise ratio is measured with a 40db. calibrated attenuator and has the value of 25:1, care being taken to avoid saturation. Thus the sensitivity of the system for D.P.P.H. is about 8×10^{16} spins at $300^{\circ}K$. At helium temperatures the sensitivity will be enhanced by the larger difference in the populations of the electronic energy levels (Section 2.2), and the above figures would indicate the minimum number of detectable spins as 1.3×10^{15} at $4.2^{\circ}K$. A value slightly better than this can be expected due to the increase in the Q-value of the cavity with decrease in temperature. For a paramagnetic sample other than

D.P.P.H. the spectrometer sensitivity may be stated as:-

$$4 \times 10^{14} \Delta H \text{ spins at } 4.2^{\circ}K.$$

where ΔH is the line width (in gauss) of the specimen under consideration. This is not high by spectrometer standards but is adequate for the studies undertaken.

4.2. Alignment Procedure.

In order to attain maximum stability the klystron and associated electronics are switched on at least one hour prior to taking any readings. The alignment procedure is as follows:-

1) Apply the voltage sweep to the reflector of the signal klystron and observe by detection on the C.R.O. that the resonant cavity dip is in the middle of the klystron mode.

2) Tune the cavity wavemeter to resonance and observe the wavemeter cavity dip superimposed on the main cavity dip.

3) The local oscillator klystron and I.F. amplifier are switched on. Adjust the reflector potential (or the mechanical tuning, if necessary) of the L.O. klystron until the I.F. response curve is obtained. The resonant cavity dip should be in the centre of the response curve.

4) Adjust the sliding stub tuner until the cavity dip is a maximum, i.e. to critical coupling.

5) Switch off the power klystron sweep and adjust the reflector voltage of this klystron until the I.F. second detector meter

indicates an output. The cavity is tuned by means of the quartz rod until this meter shows a dip.

6) Set up the A.F.C. circuit as described in Section 3.8.c) and switch in the stabilisation.

7) With the calibrated attenuators set at the required power levels the spectrometer is now set up, and the sample absorption should be observed on the C.R.O. at the required d.c. magnetic field value with the 50c/s field modulation on.

On filling the cryostat with liquid helium the cavity length has to be reduced by approximately 2.5mm. for it to have the same resonant frequency as at room temperature. The change in resonant length is mainly due to the dielectric constant of liquid helium being greater than unity. Thus, each step of the alignment procedure has to be checked after the liquid helium transfer and the system retuned where necessary.

4.3. Method of taking Readings.

With the spectrometer lined up as above and the d.c. magnetic field and field sweep on, an absorption can be observed on the oscilloscope. Once the d.c. magnetic field is set to the resonance value the magnetic sweep is switched off, and observations are made by means of the valve voltmeter. Normally the calibrated attenuators, A1 and A2, are initially set to their maximum and minimum values respectively, and the

other calibrated attenuator in the signal klystron arm ($A1^1$) is adjusted to avoid any initial saturation effects. The normal setting for this is 20db. and this remains fixed throughout the experiment.

In the continuous wave saturation method used here, the incident power on the paramagnetic sample is increased in steps by means of attenuator A1, and the resultant change in the intensity of the absorption is measured. By making preliminary adjustments of the local oscillator klystron power with the attenuator in that arm, the I.F. amplifier gain, and the sliding stub tuner to obtain the same degree of coupling for the resonant cavity, a standard reading on the valve voltmeter is achieved with the d.c. magnetic field off resonance. The crystal current meter, wavemeter, current meter and second detector meter are used to monitor these settings. When the d.c. magnetic field is brought back to its resonance value there is an increase in the reading on the valve voltmeter due to the absorption, and for every setting of the incident power (A1), the detected power (A2) is adjusted to give this new reading on the valve voltmeter. A2 is in fact giving the change in the intensity of the absorption for any change in the incident power. Any divergence from linearity for corresponding changes in the values of A1 and A2 shows the advent of saturation, and the saturation curve may be drawn from these readings.

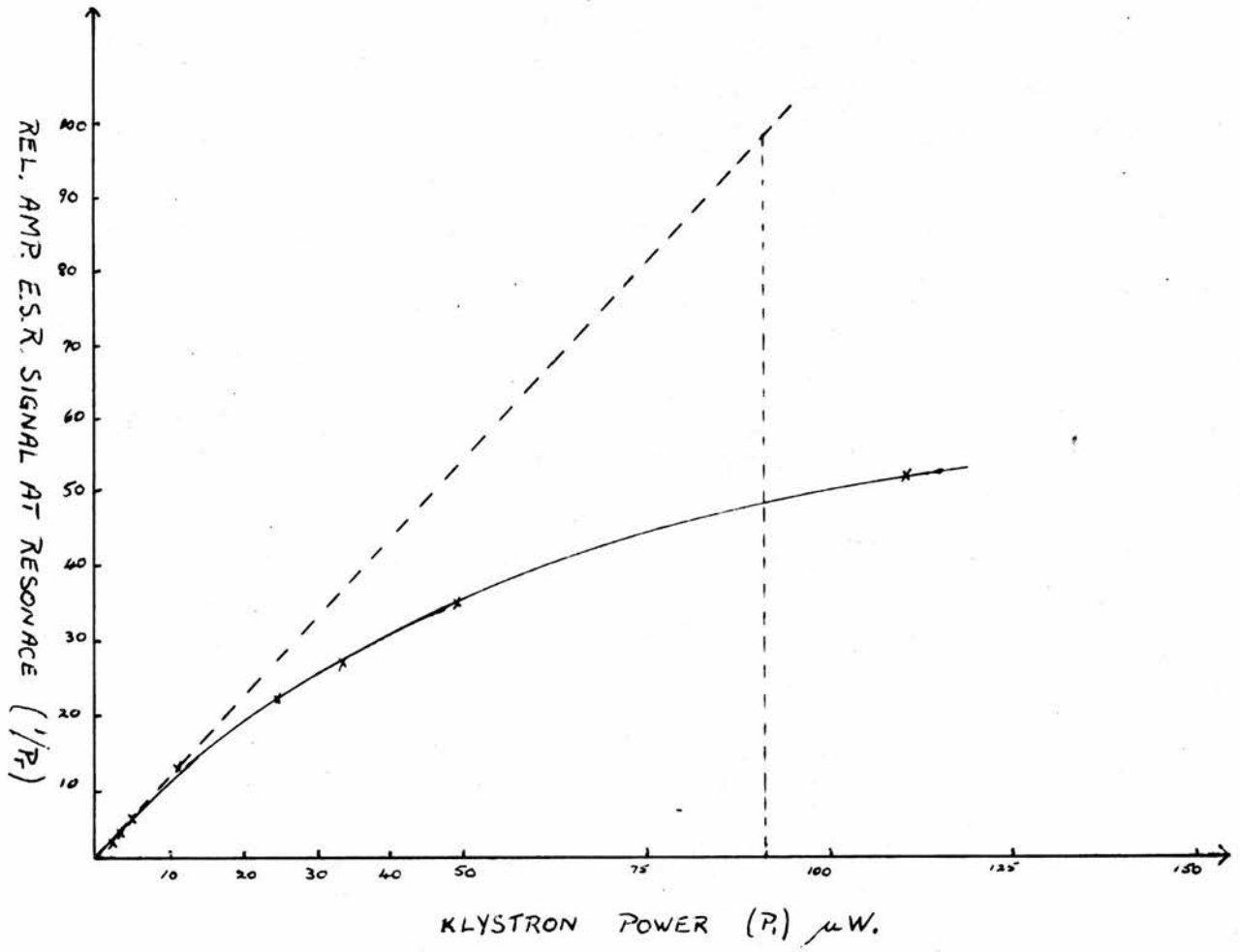

Fig. 13. Saturation Curve for D29 at 4.2°K.

Table 2.

Attenuator readings for Saturation of sample D29 at $4.2^{\circ}K$

Operating frequency = f_0 = 9375Mc/s. Attenuator $A1^1$ = 20db.

Attenuator Scale Readings		Attenuation db.		Attenuation (arbitrary units)		Klystron Power (arb.units)	W.
A1mm.	A2mm.	A1+A1'	A2	a_1	$a_2=\frac{1}{Pr}$	$P_1=\frac{1}{a_1}$	P_1
5.485	8.77	60.0	0	1.000×10^{6}	1.00	1.000×10^{-6}	0.50
5.68	8.195	56.5	1.64	4.467×10^{5}	1.46	2.238	1.12
5.88	7.805	53.0	3.71	1.995	2.35	5.012	2.51
5.96	7.555	51.65	5.46	1.462	3.52	6.839	3.42
6.058	7.325	50.0	7.39	1.000×10^{5}	5.48	1.000×10^{-5}	5.00
6.28	6.955	46.5	10.93	4.467×10^{4}	12.4	2.238	11.19
6.51	6.740	43.0	13.32	1.995	21.5	5.012	25.06
6.605	6.650	41.65	14.25	1.462	26.6	6.839	34.19
6.715	6.565	40.0	15.37	1.000×10^{4}	34.4	1.000×10^{-4}	50.00
6.972	6.420	36.5	17.14	4.467×10^{3}	51.8	2.238	111.9
7.272	6.330	33.0	18.35	1.995	69.0	5.012	250.6

In Section 2.4. the Saturation Factor was defined as

$$S = (1 + \tfrac{1}{2}\gamma^2 H_1^2 T_1 T_2)^{-1} \qquad (4.1)$$

and this may be evaluated from the saturation curve, and hence the value of the spin-lattice relaxation time T_1 if the other terms are known.

4.4. Measurement of T_1 for Diamond.

All measurements of the spin-lattice relaxation time were limited to the most concentrated of the series of neutron-irradiated diamond specimens described in Section 2.8. An observation of the resonance signal of Specimen D27 was made and it was found to be about one-tenth of that exhibited by Specimen D29. This is a very approximate estimate, both observations being carried out under the same experimental conditions. On comparison with the irradiation data given in Chapter II, it would appear that the defect creation is proportional to the neutron doseage.

A series of experiments have been completed for the sample D29 over the temperature range from 4.2°K. to 1.17°K., and the results are discussed below. A typical set of readings of the two calibrated attenuators A1 and A2, are shown in Table 2, and the corresponding saturation curve is plotted in Figure 13, the operating temperature being 4.2K. The results for the four other temperatures in the range considered are shown graphically by the saturation curves in Figures 14, 15, 16 and 17. From

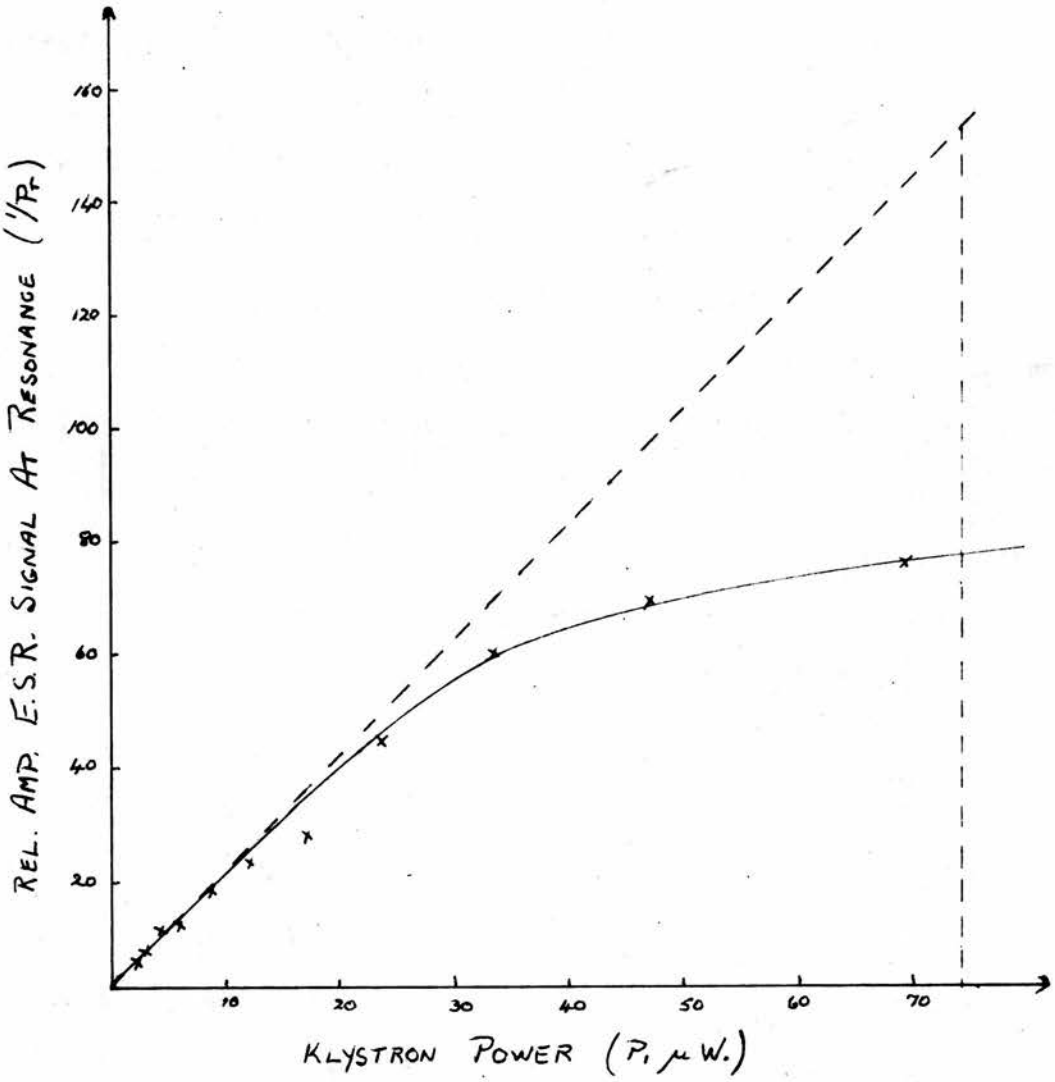

Fig. 14. Saturation Curve for D29 at 3.0°K.

these curves the saturation factor of Equation 4.1 can be obtained, and thus T_1, once T_2 and H_1 are known. At resonance it may be assumed that this saturation factor will be equal to $\frac{1}{2}$ when the measured amplitude of the spin resonance absorption is one half of the value it would have been if the system had remained linear. Thus, by drawing the tangent to the saturation curve at the low power level region, the power level at which this saturation factor is equal to $\frac{1}{2}$ can be found. It remains to evaluate T_2, the spin-spin relaxation time, and H_1, the amplitude of the rotating microwave magnetic field in the resonant cavity.

As shown in Section 2.3 the spin-spin relaxation time, T_2, may be determined from the line width of the electron spin resonance signal. Two visual methods were used to estimate the line width.

The first method was to compare the line width of the diamond line with that of a known marker using 50 c/s. magnetic field modulation. D.P.P.H. cannot be used for direct comparison as the g-values are too close, the g-value for diamond being 2.0028, and that of D.P.P.H. is 2.0036. Thus the resonance lines of the two specimens would overlap if both were contained in the same cavity. Blue plasticine with a g-value of 2.03 was used as a secondary marker (the resonance is due to sulphur impurities), the diamond line first being compared with this, and then the blue plasticine compared with D.P.P.H. The

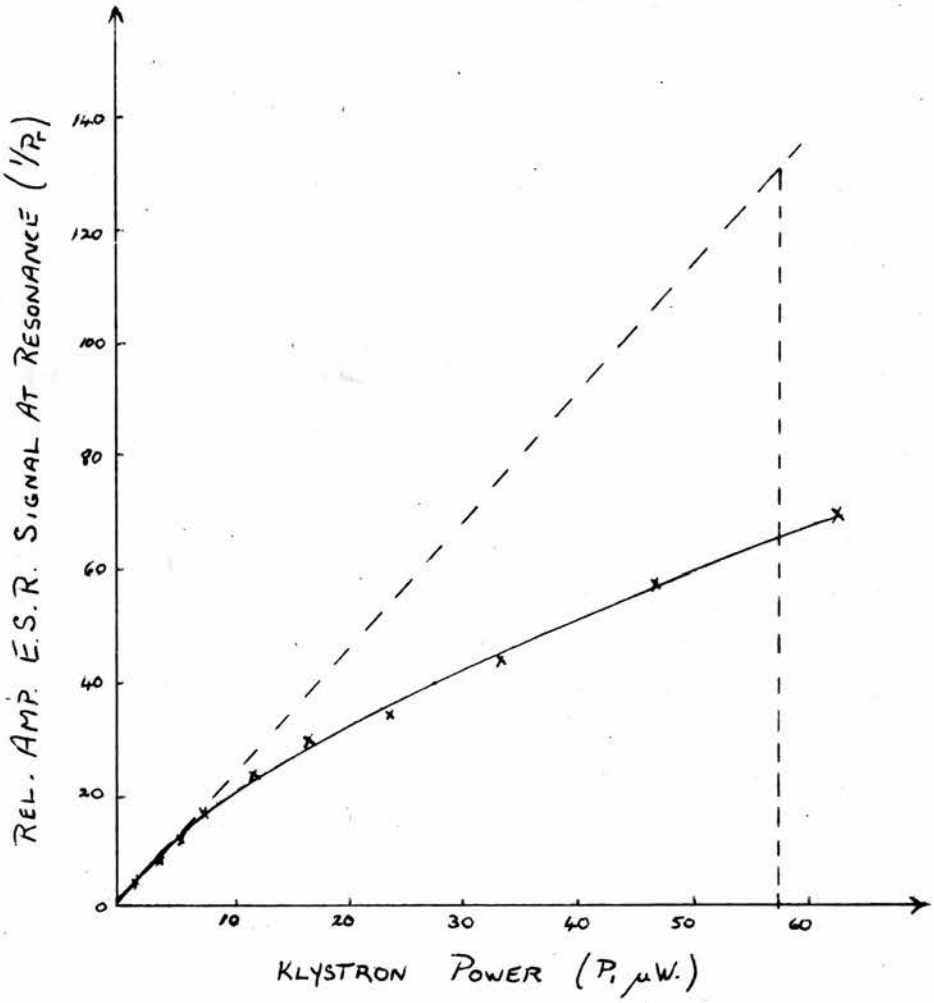

Fig. 15. Saturation Curve for D29 at 2.2°K.

D.P.P.H. has a known line width of 2.7 gauss and, from the second experiments the line width of the blue plasticine sample was found to be ~8 gauss[60]. The diamond line width was estimated to be ~7.5 gauss at liquid helium temperatures.

The alternative method employed to measure the diamond resonance line width was to take a known fraction of 50 c/s. magnetic field sweep voltage, phase shift this by 90°, and apply it synchronously to the X-plates of the oscilloscope (Figure 19a). Thus the width of the trace on the oscilloscope is known in gauss from the sweep coil characteristics (Section 3.6.c)) and the line width of the resonance line may be read off directly. This is estimated as ~7 gauss, and this value is used in the following calculation for the line width at liquid helium temperatures. The value for a comparable sample as quoted by Griffiths[40] at 90°K. is 26 gauss.

Thus T_2 can be determined, but to evaluate T_1 it is still necessary to calculate the amplitude (H_1) of the microwave magnetic field at the specimen. Portis[14] expresses H_1^2 in the form

$$H_1^2 = 32\pi Q_u(1 - |\Gamma|^2)\frac{P}{\omega V}$$

where Q_u = unloaded Q of the resonant cavity

$|\Gamma|^2$ = power reflection coefficient of the cavity

P = power incident on the cavity (ergs)

ω = operating frequency (radians/sec)

V = volume of the resonant cavity.

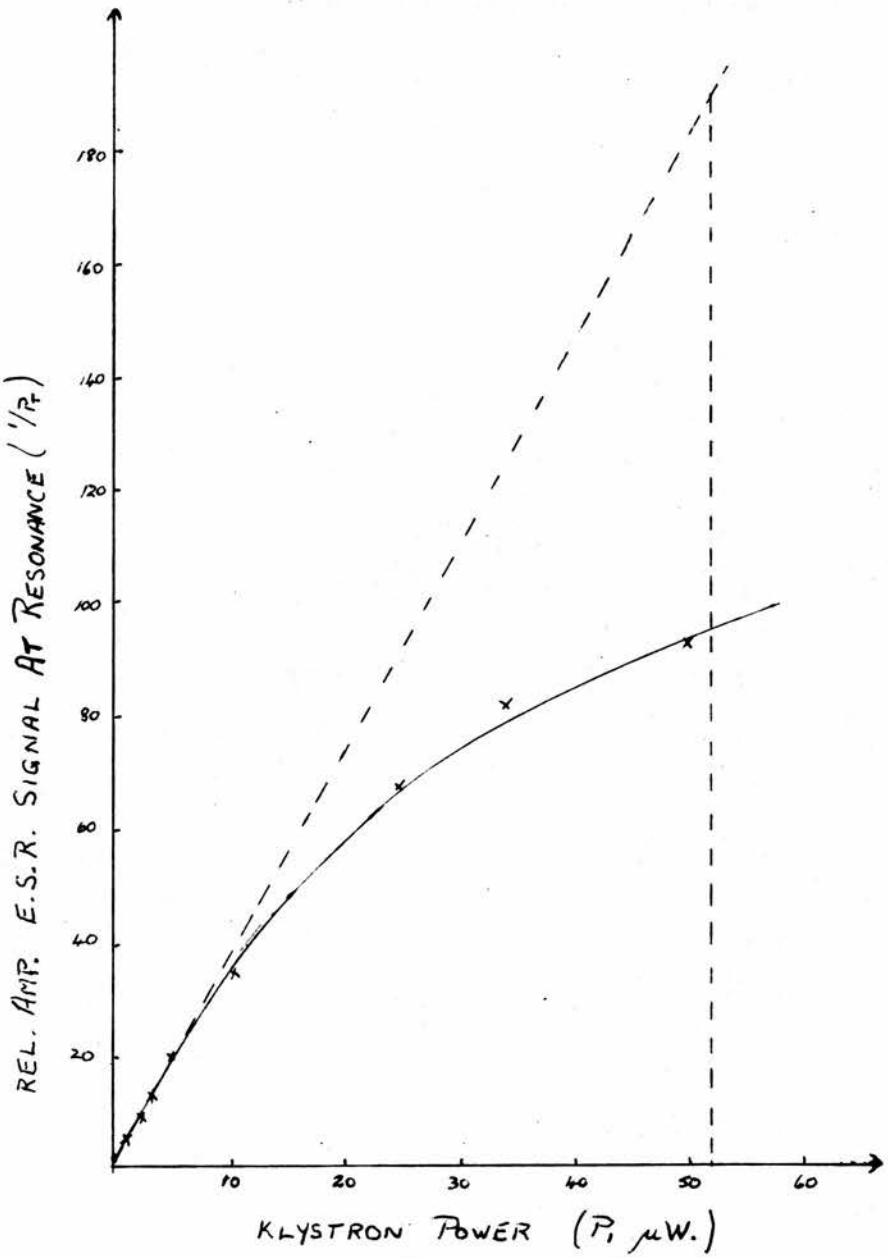

Fig. 16. Saturation Curve for D29 at 1.7°K.

As mentioned in Section 3.5.c) the Q-value of the cavity is found by inserting a standing wave indicator in the cavity arm of the microwave bridge. From the V.S.W.R. readings at 4.2 K°.,

Unloaded Q = Q_u = 10^4

Loaded Q = Q_L = 6,500

V.S.W.R. = τ = 0.54

Power reflection coefficient $|\Gamma|^2$ = 0.09.

Other data required is:-

$$\omega = 2\pi \times 0.9375 \times 10^{10} \text{ radians/sec.}$$

$$V = \pi r^2 h = 11.5 \text{ cc.}$$

$$H_1^2 = \frac{32\pi \times 10^4 \times 0.91}{2\pi \times 0.9375 \times 10^{10} \times 11.5}$$

$$= 1.35 \times 10^{-6} \text{ (gauss)}^2/\text{erg.}$$

$$= 1.35 \times 10^{-5} \text{ (gauss)}^2/1\,\mu\text{w. incident microwave power}$$

This value gives very close agreement with that worked out by Campbell[60] for an identical cavity using the energy stored in the cavity and the field equations for the mode of operation.

Using the above values of H_1^2 and T_2, and the gyromagnetic ratio $\gamma = 2\pi \times 2.8 \times 10^6$ radians/sec/gauss, the saturation factor may be evaluated:-

$$(1 + \tfrac{1}{2}\gamma^2 H_1^2 T_1 T_2)^{-1} = \tfrac{1}{2}$$

$$\therefore\ T_1 = \frac{4}{\gamma^2 H_1^2 T_2}$$

$$= \frac{5.90 \times 10^{-2}}{P} \text{ sec.}$$

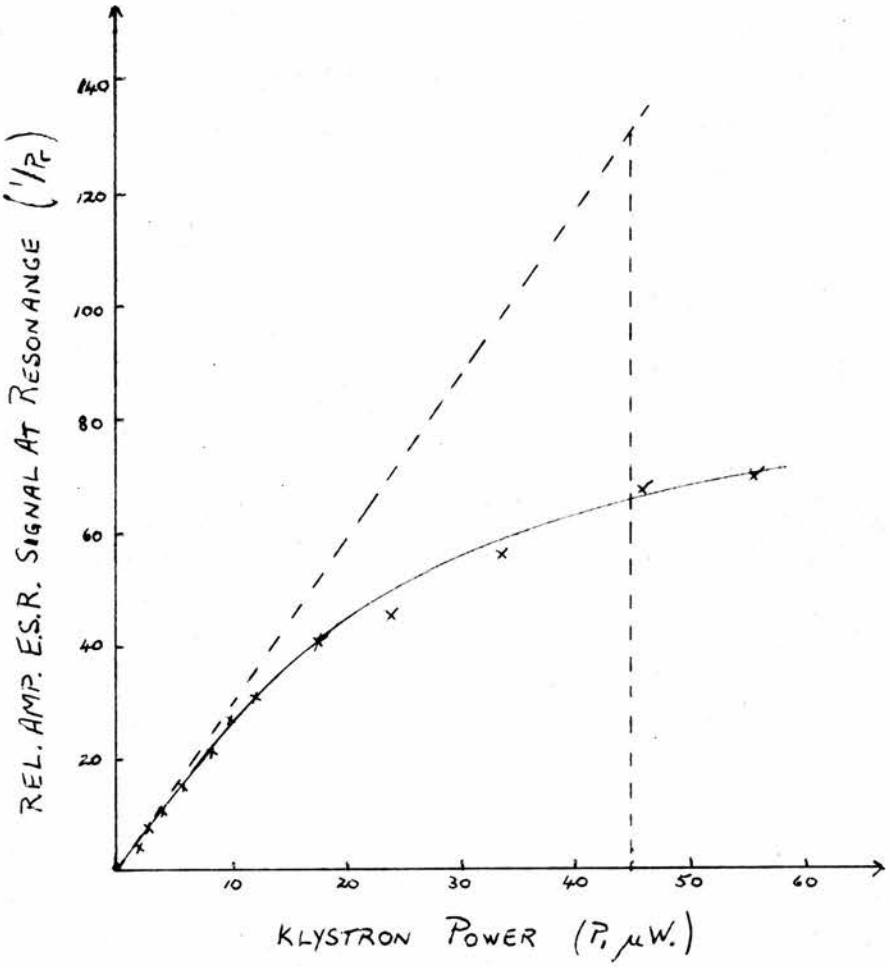

Fig. 17. Saturation Curve for D29 at 1.17°K.

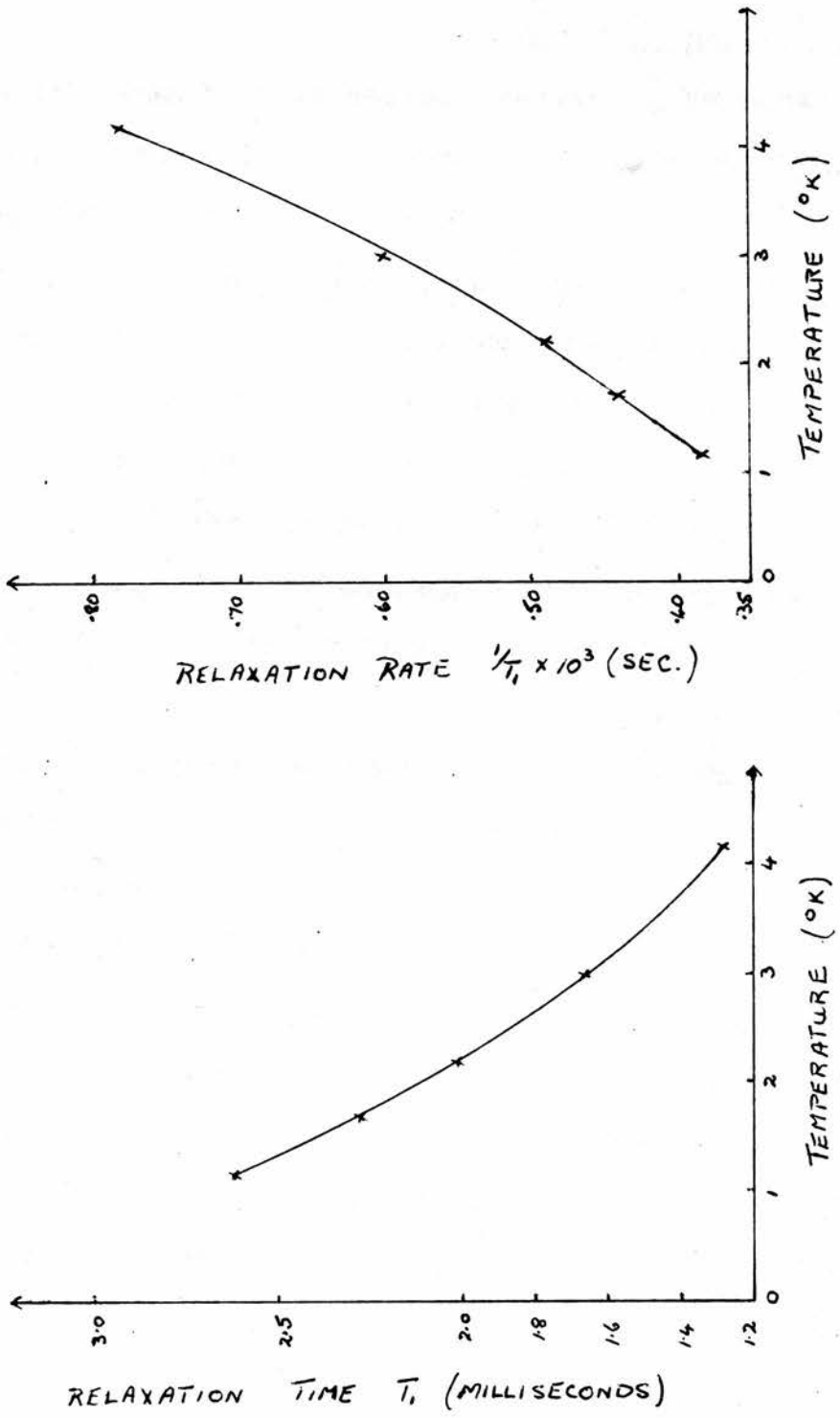

Fig. 18. Temperature Dependence of Relaxation Effect.

P is the power incident on the cavity (in microwatts) when the saturation factor, S, is equal to $\frac{1}{2}$, but the value as measured by the attenuator A1 and given by the respective saturation curves is twice this due to the splitting of power at the bridge magic tee, assuming this is matched. The results from figures 13, 14, 15, 16 and 17 of the saturation curves and required power value at the various temperatures are detailed in Table 3.

Table 3.

Temperature	4.2	3.0	2.2	1.7	1.17°K
Klystron Power for S = $\frac{1}{2}$	92	71	58	52	45 microwatts
Incident Power, P_1	41	35.5	29	26	22.5 microwatts
Relaxation Time, T_1	1.28	1.66	2.03	2.27	2.62 milliseconds
Relaxation Rate, $\frac{1}{T_1}$	0.78	0.60	0.49	0.44	0.38 x 10^3 sec.$^{-1}$

4.5. Interpretation of Results.

The graph of $\frac{1}{T_1}$ against temperature (Figure 18) shows the inverse dependence of the spin-lattice relaxation time on temperature in the range covered, and at the lowest temperature the graph appears to approach linearity which is in agreement with the hypothesis that the direct process of phonon interaction between the spins in the electronic energy states is the dominant one (Section 2.5.). At the higher temperatures the curve is non-linear tending to a higher order inverse dependence of the relaxation time on temperature, which might indicate that the Raman type mechanism is beginning to affect the relaxation process.

The temperature range is not wide enough, nor are the number of temperatures at which results are taken large enough, for any direct conclusion to be made about the power of the inverse temperature dependence, or where one mechanism predominates over the other. We can say that the results indicate that the direct mechanism is stronger the lower the operating temperature, and at higher temperatures the Raman mechanism will take over completely the process of re-establishing the thermal equilibrium of the spin system.

4.6. The Diamond Spectrum.

In addition to the main diamond resonance line many other resonance lines of order 100 times smaller were observed over a

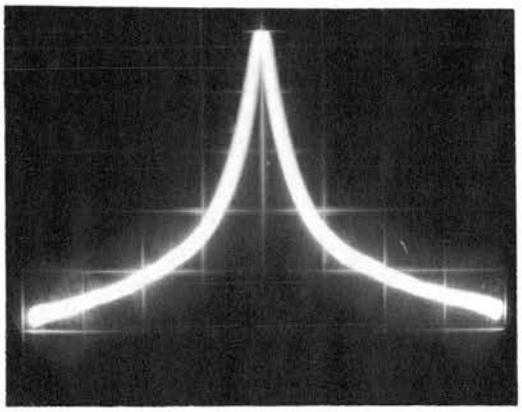

a) D29 Resonance at 4.2°K.

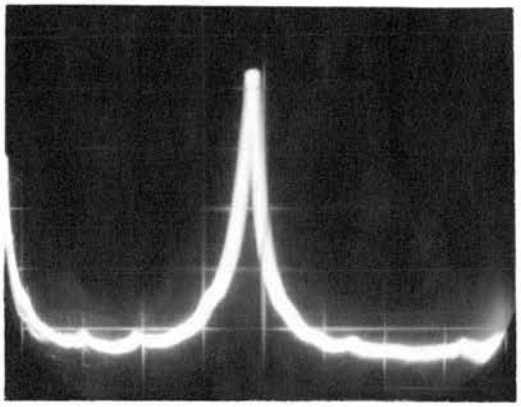

b) D29 Resonance with Two Satellites at 1.17°K.

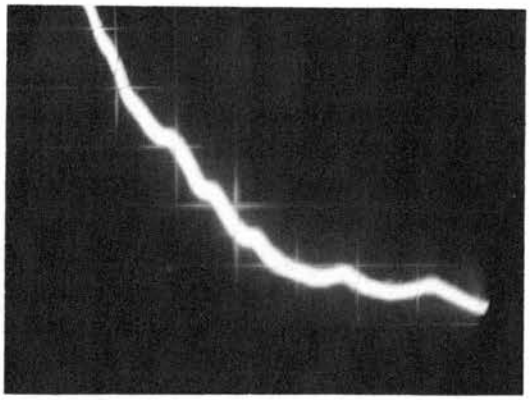

c) D29 Resonance with Satellites superimposed on Main Line at 1.17°K.

Figure 19.

range in d.c. magnetic field from 4,500 gauss to 2,750 gauss. In all about 30 other lines were observed. Griffiths et al.[40] attribute twelve satellite lines to the different orientations of the possible C_2 molecule, but the majority of the lines observed must be due to impurity centres. Smith, Gelles and Sorokin[61] attribute the weak lines ($\Delta H \sim \frac{1}{3}$ gauss) observed by them to bound aluminium acceptors, but the pattern of this spectrum will vary from sample to sample. The number of lines observed is dependent on the orientation of the crystallographic axes with respect to the d.c. magnetic field. The applied 50c/s modulation field sweep is not wide enough to give a visual display of the whole spectrum, but some of these lines are shown in Figure 19 b) and 19 c).

From the calibration of the sensitivity of the spectrometer and the observed amplitude and line width of the main line of the C.29 diamond spectrum, the number of spins in the specimen is estimated to be approximately 10^{16} spins.

4.7. Spectrum of Neutron-Irradiated Magnesium Oxide.

Samples of neutron-irradiated MgO were obtained for the maser experiment in this laboratory [60]. The electron spin resonance due to the F-centres induced by the irradiation has a main central resonance line and hyperfine pattern of six spectral lines due to the nuclear spin value $\frac{5}{2}$ of the neighbouring Mg^{25} atoms. Other orientations of the Mg^{24} and

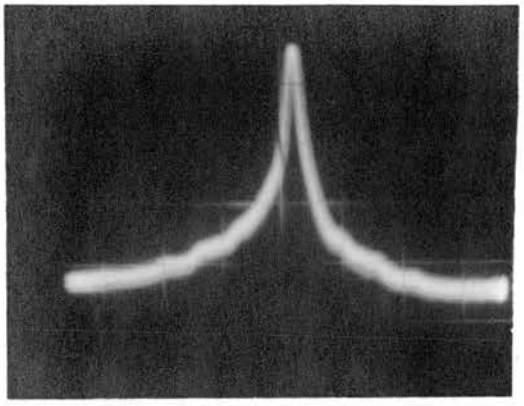

a) MgO Resonance at Room Temperature.

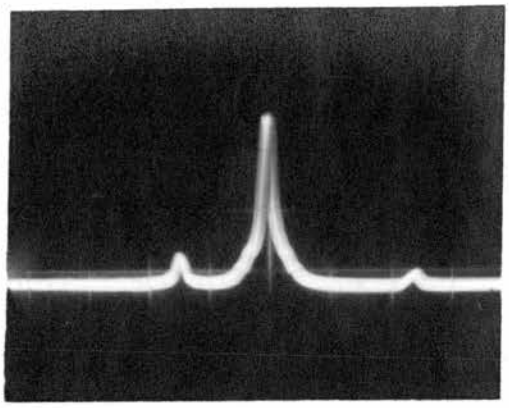

b) MgO Resonance with Two Satellites at 4.2°K.

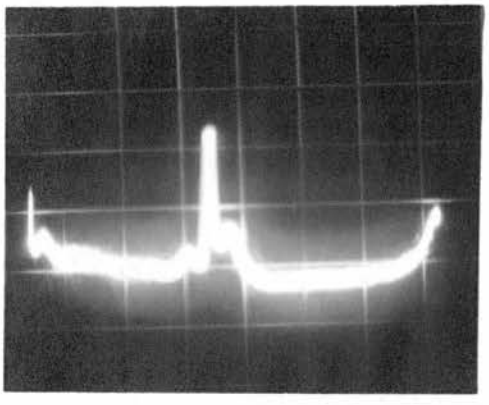

c) Typical MgO Satellite at 1.17°K.

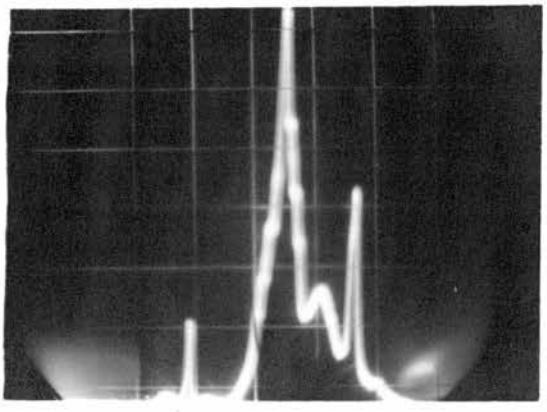

d) MgO Resonance with Satellites superimposed on Main Line at 1.17°K.

Figure 20.

Mg^{25} nearest neighbours occur and give different resonance spectra. Maser amplification and oscillation have been observed with these samples, and the spin-lattice relaxation time has been estimated as about 4 milliseconds at 4.2°K.

Attempts to measure this relaxation time by the continuous wave saturation method were unsuccessful due to early saturation of the spin system. It would be necessary to operate at very low incident powers producing higher system instability if this was to be avoided. Some observations were made on the spectrum of the MgO samples.

A strong central resonance line was observed, (with a g-value approximately the same as for a free electron) and six satellite lines of amplitude roughly 10% of the main line. These were placed asymmetrically about the main line and, on increasing the video gain on the oscilloscope, appeared as six sets of triplets. Again the 50c/s field modulation is not large enough to display the whole spectrum, but Figure 20 b) shows the main line and the first satellite on each side of this central line, the operating temperature being 4.2°K. Figure 20 c) shows a typical satellite as a triplet, again asymmetrical in structure At 1.2°K. many more narrow lines of very much smaller intensity appeared, and these may be attributed to some paramagnetic impurity, as in the case of the diamond resonance. These are shown in Figure 20 d).

No attempt has been made here to explain this spectrum, but it has been studied by a number of research workers (62). The number of spins in the specimen was estimated as in the order of 10^{18} per cc.

4.8. Conclusions and Recommendations.

By this method the spin-lattice relaxation time has been measured for a specimen of neutron-irradiated diamond, and an indication of the correct temperature dependence in the range from 1.2°K. to 4.2°K. has been found. Thus it would appear that similar observations could be made on any specimen of a comparable size and density of paramagnetic centres, if the relaxation time is of the order of milliseconds. Longer or shorter relaxation times might produce further operational difficulties. The other samples available in the series of neutron-irradiated diamonds should now be examined for any concentration dependence of the spin-lattice relaxation effect. A better interpretation of the results might be achieved by expressing the relationships between the attenuator readings, as the incident power is increased until saturation, in terms of other variables so that the relaxation time may be calculated from a saturation graph without drawing tangents or making other approximations.

The apparatus could be improved further by the use of a resonant cavity with a higher Q-value. A rectangular cavity operating in the TE 102 mode has proved satisfactory in other experiments in the laboratory, and the quartz rod fine tuning can be retained. Stabilisation of the signal klystron would help greatly to the ease of operation, but the large power range covered in the course of determining the saturation characteristics presents a difficulty if the klystron is to be locked to the resonant frequency of the cavity.

Although this method gives adequate results, the methods using pulsed saturation or inversion of the spin system appear to give a better indication of the actual mechanisms involved in the relaxation process. They also give a visual presentation of the relaxation rate, and are thus more suited to show any anomolies which may occur.

APPENDIX

Principal Microwave Components

Signal Klystron	Varian, X-13
Local Oscillator Klystron	English Electric, K302
Sliding Stub Tuners	Microwave Instruments Limited, 32/1400
Ferrite Isolators	M.I.L., 32/4010
40db. Calibrated Attenuators (A1 and A2)	M.I.L., 32/635
40db. Calibrated Attenuator ($A1^1$)	M.I.L., 32/630
Variable Attenuator	M.I.L., 32/670
Cavity Wavemeter	M.I.L., 32/2000
Bridge Magic Tee	Philips, PP4050X
Directional Coupler	M.I.L., 32/1700
Adjustable Crystal Holder	Philips, PP4220X
Flexible Waveguide Section	Sanders, FG16-6PC

REFERENCES

1. I. Waller, Z. Phys., 79, 370 (1932)
2. C.J. Gorter, "Paramagnetic Relaxation" (Elsevier, Amsterdam 1947)
3. L.E. Alsop, J.A. Giordmaine, C.H. Mayer and C.H. Townes, Paris Symposium on Radio Astronomy. (Stanford University Press, 1959)
4. T.A. Matthews, "Quantum Electronics", (Columbia University Press, 1960)
5. E. Zavoisky, J. Phys. U.S.S.R., 9, 211 (1945)
6. A.H. Cooke, Rep. Prog. Phys., 13, 276 (1950)
7. N. Bloembergen, E.M. Purcell and R.V. Pound, Phys. Rev., 73, 679 (1948)
8. B. Bleaney and K.W.H. Stevens, Rep. Prog. Phys., 16, 108 (1953)
9. K.D. Bowers and J. Owen, ibid., 18, 364 (1954)
10. D.J.E. Ingram, "Free Radicals as studied by Electron Spin Resonance", (Butterworths Publications Ltd 1958)
11. D.M.S. Bagguley and J. Owen, Rep. Prog. Phys., 20, 304 (1957)
12. J.H. Van Vleck, Phys. Rev., 74, 1168 (1948)
13. M.H.L. Pryce and K.W.H. Stevens, Proc. Phys. Soc.,A, 63, 36 (1950)
14. A.M. Portis, Phys. Rev., 91, 1071 (1953)
15. F. Bloch, ibid., 70, 460 (1946)
16. E.R. Andrew, "Nuclear Magnetic Resonance", (Cambridge University Press, 1955)
17. W. Heitler and E. Teller, Proc. Roy. Soc., A, 155, 629 (1936)
18. M. Frierz, Physica, 5, 433 (1938)
19. R. de L. Kronig, ibid., 6, 33 (1939)
20. C.J. Gorter, P. Teunissen, and L.J. Dijkstra, ibid., 5, 1013 (1938)

21. W.J. de Haas and F.K. Du Pré, ibid., 5, 969 (1938)
22. H.B.G. Casimer and F.K. Du Pré, ibid., 5, 507 (1938)
23. P. Debye, Phys. Z., 39, 616 (1938)
24. J.H. Van Vleck, Phys. Rev., 57, 426 (1940)
25. H.N.V. Temperley, Proc. Camb. Phil. Soc., 35, 256 (1939)
26. D. Bijl, Thesis, Leiden (1950)
27. J.H. Van Vleck, Phys. Rev., 59, 724 (1941)
28. M.W.P. Strandberg, ibid., 110, 65 (1958)
29. P.W. Anderson, ibid., 114, 1002 (1959)
30. T. Holstein, ibid., 72, 1212 (1947; 83, 1159 (1951)
31. J.A. Giordmaine, L.E. Alsop, F.R. Nash and C.H. Townes, ibid., 109, 302 (1958)
32. M.W.P. Strandberg, C.F. Davis, B.W. Faughnan, R.L. Kyhl, and G.J. Wolga, ibid., 109, 1988 (1958)
33. N. Bloembergen, S. Shapiro, P.S. Persham and J.O. Artman, ibid., 114, 445 (1959)
34. J.H. Van Vleck, "Quantum Electronics", (Columbia University Press, 1960)
35. A.H. Eschenfelder and R.T. Weidner, Phys. Rev., 92, 869 (1953)
36. G. Feher and H.E.D. Scovil, ibid., 105, 760 (1957)
37. A.L. McWhorter and J.W. Meyer, ibid., 109, 312 (1958)
38. C.F. Davis, Jr., M.W.P. Strandberg and R.L. Kyhl, ibid., 111, 1268 (1958)
39. K.D. Bowers and W.B. Mims, ibid., 115, 285 (1959)
40. J.H.E. Griffiths, J. Owen and I.M. Ward, a) Nature, 173, 439 (1954); b) "Defects in Crystalline Solids", P.81 (London: Physical Society, (1955)
41. R.A. Dugdale, Brit. J. Appl. Phys., 4, 334 (1953)
42. M.C.M. O'Brien and M.H.L. Pryce, "Defects in Crystalline Solids", P.88. (London: Physical Society, 1955)

43. C.D. Clark, R.W. Ditchburn and H.B. Dyer, Proc. Roy. Soc., A, 237, 75 (1956)

44. G. Feher, Bell Syst. Tech. J., 36, 449 (1957)

45. G.L. Ragan, M.I.T., Radiation Laboratory Series (McGraw - Hill), Vol.9, Ch.8

46. C.G. Montgomery, ibid., Vol.11, P.527

47. R.V. Pound, ibid., Vol.16, P.259

48. H.C. Torrey and C.A. Whitmer, ibid., Vol.15, P.353

49. H. Van Dijk and M. Durieux, Physica, 24, 920 (1958)

50. R. Berman, Phil. Mag., 42, 642 (1951)

51. I.G. Wilson, C.W. Schramm and J.P. Kinzer, Bell Syst. Tech. J., 25, 408 (1946)

52. C.G. Montgomery, M.I.T. Radiation Laboratory Series, (McGraw - Hill), Vol.11, P.297

53. C.G. Montgomery, ibid., Vol.11, P.333

54. E.L. Grinzton, "Microwave Measurements" (McGraw - Hill) P.406

55. G.C. Lowe, Electronic Engineering, 31, 138 (1959)

56. G.E. Valley and H. Wallman, M.I.T. Radiation Laboratory Series, (McGraw - Hill), Vol.18

57. R.V. Pound, ibid., Vol.16, 302

58. S.N. Van Voorhis, ibid., Vol.23, 35

59. D.J.E. Ingram, "Spectroscopy at Radio and Microwave Frequencies", (Butterworths Publications Ltd. 1955)

60. C.K. Campbell, Thesis, St Andrews (1960)

61. W.V. Smith, I.L. Gelles and P.P. Sorokin, Phys. Rev. Letters, 2., 39, (1959)

62. J.E. Wertz, P. Auzins, R.A. Weeks and R.H. Silbee, Phys. Rev., 107, 1535 (1957)

ACKNOWLEDGMENTS.

I should like to express my sincere thanks to -

Professor J.F. Allen, F.R.S.	for his interest and the facilities of the Physical Laboratory of the University of St Andrews.
Dr D. Bijl, F.R.S.E.	for his supervision and his helpful advice.
Dr C.K. Campbell, Messrs I.M. Brown and C.B. Taylor	for their share in the design and testing of much of the equipment in the microwave section of the Laboratory.
Mr J. Gerrard	for his assistance with the photographs, and in ordering equipment.
Mr R.H. Mitchell	for his uncomplaining efforts to maintain a plentiful supply of liquid helium.
Messrs J. McNab, T. Marshall, M. Bird, G. Dunsire and F. Akerboom	for their excellent work on the equipment.
Mr H. Cairns	for his assistance with electrical components.
Miss E. Cole	for typing this thesis.
Sir James Caird's Travelling Scholarships Trust, and The University of St Andrews	for the award of a scholarship and a maintenance grant.